PNNL-11981
UC-2030

Pacific Northwest National Laboratory

Operated by Battelle for the
U.S. Department of Energy

Mechanisms of Gas Retention and Release: Experimental Results for Hanford Single-Shell Waste Tanks 241-A-101, 241-S-106, and 241-U-103

S. D. Rassat
S. M. Caley
P. R. Bredt
P. A. Gauglitz
D. E. Rinehart
S. V. Forbes

September 1998

Prepared for the U.S. Department of Energy
under Contract DE-AC06-76RLO 1830

PNNL-11981

DISCLAIMER

PACIFIC NORTHWEST NATIONAL LABORATORY
operated by
BATTELLE
for the
UNITED STATES DEPARTMENT OF ENERGY
under Contract DE-AC06-76RLO 1830

Printed in the United States of America

Available to DOE and DOE contractors from the Office of Scientific and Technical Information, P.O. Box 62, Oak Ridge, TN 37831; prices available from (615) 576-8401.

Available to the public from the National Technical Information Service, U.S. Department of Commerce, 5285 Port Royal Rd., Springfield, VA 22161

This document was printed on recycled paper.
(9/97)

PNNL-11981
UC-2030

Mechanisms of Gas Retention and Release: Experimental Results for Hanford Single-Shell Waste Tanks 241-A-101, 241-S-106, and 241-U-103

SD Rassat
SM Caley
PR Bredt
PA Gauglitz
DE Rinehart
SV Forbes

September 1998

Prepared for
the U.S. Department of Energy
under Contract DE-AC06-76RLO 1830

Pacific Northwest National Laboratory
Richland, Washington 99352

Executive Summary

The 177 underground waste storage tanks at the Hanford Site contain millions of gallons of radioactive waste resulting from the purification of nuclear materials and related processes. Through various mechanisms, flammable gas mixtures of hydrogen, ammonia, methane, and nitrous oxide are generated and retained in significant quantities within the waste in many (~25) of these tanks. The potential for large releases of retained gas from these wastes creates a flammability hazard. It is a critical component of the effort to understand the flammability hazard and a primary goal of this laboratory investigation to establish an understanding of the mechanisms of gas retention and release in these wastes. The results of bubble retention experimental studies using waste samples from several waste tanks and a variety of waste types support resolution of the Flammable Gas Safety Issue. Gas bubble retention information gained in the pursuit of safe storage will, in turn, benefit future waste operations including salt-well pumping, waste transfers, and sluicing/retrieval.

Waste Samples

Previous laboratory studies on simulated and actual wastes established a framework within which to classify gas bubble retention mechanisms. The behavior observed in earlier gas retention experiments on four Hanford double-shell tank (DST) wastes (241-AN-103, 241-AW-101, 241-SY-101, and 241-SY-103) and one single-shell tank (SST) waste (241-S-102) is captured within this general framework. Considering the relatively large number (19) of SSTs on the Hanford Flammable Gas Watch List, the experimental study of SST waste gas retention and release is limited. To answer this, the current gas retention experiments were conducted on four samples from three Hanford SSTs (one each from 241-A-101 and 241-S-106 and two from 241-U-103). These SSTs were selected using several criteria, including diversity of waste classification (type), behavior indicating that the waste retains, or has the potential of retaining, significant quantities of gas, status of supporting flammable gas data (e.g., retained gas sampler [RGS] results), and sample availability.

Tank 241-A-101 (A-101) is of interest because RGS results indicate that the waste exists in an unexpected configuration, with the nonconvective (solids-containing) layer on top of the convective (liquid) layer. Tank A-101 contains double-shell slurry feed waste type, and it is reported to consist primarily of saltcake. The sample tested (Core 154, segment 5) was previously used (spent) in RGS testing.

Tank 241-S-106 (S-106) contains noncomplexed waste type and is characterized as predominantly saltcake waste. This tank was of interest because barometric pressure evaluation (dL/dP) showed high gas retention (15-19%) while the majority of RGS measurements showed a maximum of 10%. The S-106 gas retention sample was from the upper half of Core 183, segment 8.

Tank 241-U-103 (U-103) also contains noncomplexed waste type but is reported to have a significant fraction of salt slurry and sludge in addition to saltcake. Two U-103 composite

samples were tested: the one identified in this study as the upper-tank composite was a mixture of samples from segments 1 and 2 (near the waste surface, Core 182); the middle-tank composite was a mixture of segments 5 and 6 (Core 182) samples. RGS measurements in a different U-103 core showed significantly more retained gas in the upper-tank segments (1–3) than in lower-tank segments (4–10); this is why two U-103 samples were selected.

Experimental Objectives and Approach

The specific objective of this work was to investigate gas retention and release in a variety of waste types using established experimental techniques that, as accurately and reasonably as possible, reflect the actual tank conditions. In addition, waste sample shear strengths and densities were measured because they can influence the mechanism and magnitude of gas retention. The existing gas retention experimental method uses a relatively small waste sample (~50–75 mL) settled in a transparent vessel. Gas bubbles are nucleated and grown over about a day by applying a vacuum to the sample in a controlled manner. Retained gas volumes are quantified by following changes in waste height, and retained gas bubble shapes and sizes are observed, providing additional qualitative information on the mechanisms of gas retention. Only a single retention analysis of a given waste type was conducted because previous studies have shown the results to be reproducible. The tests were conducted near the reported tank temperatures. The S-106 and U-103 waste samples were held at the ambient hot cell temperature (26–30°C), and the A-101 sample was maintained at ~53°C by recirculating water through a transparent water jacket. Unlike previous tests, the samples were not pre-irradiated with a gamma source to create an initial gas volume. It was predicted, and shown experimentally, that, even without pre-irradiation, enough gas was present in the samples to attain maximum retention using only the vacuum system.

Gas Retention and Release Mechanisms

The results of the gas retention experiments on the variety of wastes that are the subject of this report are in accord with existing gas retention and release models. The two predominant mechanisms of bubble retention in typical waste configurations are interstitial liquid-displacing bubbles retained by capillary forces in coarse particulate material and particle-displacing bubbles retained by the yield strength in continuum or fine particulate material. In these SST experiments on both the very fine-particulate U-103 composite samples and the relatively coarse, but still fine-grained moist salt (saltcake) wastes, A-101 and S-106, gas was retained in particle-displacing bubbles. The properties (e.g., particle size and waste depth) of the saltcake waste samples were not conducive to the formation of interstitial liquid-displacing bubbles.

Gas release mechanisms in the experimental samples were also investigated. In a typical SST configuration, in which a supernatant liquid layer is thin to nonexistent, neutral buoyant displacement is not a viable mechanism of gas release, as it is in DSTs. In the current experiments, residual supernatant liquid was removed from the SST waste samples, and gas release was characterized by changes in retained gas fractions with continued gas generation

(reduced pressure). The characteristics of these gas retention profiles were compared with previous experimental results obtained for bentonite clay simulated wastes of known strength to evaluate gas release mechanisms.

Particle-displacing bubbles demonstrate a range of behavior, evidenced in bubble shapes, that depend on the surface tension of the medium, the bubble size, and the waste strength. Assuming negligible variation in surface tension in the waste materials, the shapes of bubbles of a given size are primarily a function of the waste strength. The strength of the material, in turn, affects the mechanism of gas release, as was established in previous studies with bentonite clay simulated wastes. In sufficiently weak wastes (e.g., <10 Pa), individual or small groups of round bubbles of sufficient size overcome the strength of the material to rise to the surface and release. At intermediate strength (e.g., ~30–100 Pa), distorted round bubbles establish connected paths to the waste surface only after attaining a sufficient and relatively high gas fraction. A partial release of gas allows the surface to heal until the bubble path is reestablished through continued gas generation and/or bubble migration. In even stronger materials (e.g., ~1,000 Pa), highly distorted and elongated dendritic bubbles connect to the surface at relatively lower gas fraction, and the strength of the material is sufficient to maintain a continual release pathway.

Experimental Results

The retained bubble shapes and gas retention profiles of the A-101, S-106, and U-103 SST waste samples were all consistent with bentonite clay simulated waste samples having shear strengths on the order 50 Pa. In addition, visual observations of the hand-mixed (sheared) tank waste samples as they were being transferred (poured) to the retention vessels suggest that the strengths were less than 100 Pa. These estimated strengths are an order of magnitude less than shear strengths measured on the as-received samples before they were mixed and transferred to the retention vessels. The average shear strengths of two to four replicate analyses were 640 Pa in A-101, 1,100 Pa in S-106, 750 Pa in U-103 upper-tank composite, and 4,500 Pa in U-103 middle-tank composite. All shear strength measurements were made at the ambient hot cell temperature (~28°C) except for the A-101 sample, which was measured at ~55°C. The discrepancies in measured shear strengths and in situ (retention vessel) estimated strengths are likely due to the shear history resulting from sample transfer and possibly due to fundamental differences in the strengths represented by the measurement techniques. The shear strengths of two additional S-106 samples (not used in gas retention testing) were measured: 1,800 Pa was determined in a Core 183, segment 9 lower half sample (adjacent to the gas retention test sample); and 16,000 Pa was determined in a Core 184, segment 4 upper half sample. The extremely high strength of this last sample is presumably due to the crystallized state of the material.

Gas retention experiments produce quantitative measures of the maximum gas fractions that can be retained by waste samples. Maximum gas fractions are determined from the maximum growth in sample volume resulting from evacuation and the estimated initial gas bubble volume (preceding evacuation). As a group, the relatively coarse grained A-101 and S-106 saltcake samples indicated higher initial retained gas fractions than the very fine-particulate U-103

samples: 0.06 initial in A-101, 0.08 initial in S-106 and 0.02 initial in both U-103 upper-tank composite and U-103 middle-tank composite. The initial gas content results, in part, from gas bubble entrainment in the vessel loading process. In the case of A-101, thermal cycling of the sample is proposed to explain the relatively high initial gas fraction. The maximum retained gas fraction varied from 0.30 to 0.51 in the four samples tested: 0.40 in A-101, 0.51 in S-106, 0.30 in U-103 upper-tank composite, and 0.42 in U-103 middle-tank composite. The relatively low maximum retention in the U-103 upper-tank composite (0.30 gas fraction) may be due to a pressure control correction made during the experiment; or it may be the result of differences in the two composite samples that were not readily identified.

Interestingly, the measured maximum gas fraction in the U-103 middle-tank composite sample (0.42) is in good agreement with a reported x-ray analysis (0.47 gas fraction) of segment 4 (Core 182), which is located immediately above the gas retention sample segments. This suggests that a near-maximum retention condition may exist in this portion of the tank. In A-101 tests, the measured 0.40 maximum gas fraction was considerably higher than the reported RGS measurement (0.14) on the same waste segment. Note, however, that RGS results provide a measure of the in situ retained gas fraction, not the maximum gas content that could be retained. A-101 gas retention sample density measurements (supernatant liquid: 1.61 g/mL; bulk waste at 0.06 gas fraction: 1.71 g/mL) indicate that the waste would have become neutrally buoyant at a gas fraction of 0.12 or greater if enough supernatant liquid had been present in the sample. This is consistent with the reported inverted waste configuration in Tank A-101 and suggests that more gas could possibly be retained in the floating solids layer.

On reaching maximum retention, the samples continued to be evacuated to observe gas releases. A very rapid and relatively large gas release was detected in the S-106 experiment. Consistent with the behavior of moderately weak (~30 Pa) bentonite clay simulated wastes, the gas fraction in the S-106 sample dropped rather suddenly from near 0.5 to about 0.3 as more than 50% of the retained gas volume was released. The S-106 retained gas fraction then held steady or increased slightly for the remainder of the test. The gas releases in A-101 and U-103 samples were more characteristic of somewhat stronger (~70 Pa) bentonite clay simulated wastes; the releases were smaller and more gradual. In the A-101 experiment, approximately 15% of the retained gas volume was released and the retained gas fraction dropped less than 0.04. The release behavior in the U-103 samples was generally intermediate of the S-106 and A-101 samples, although the data are complicated by pressure control corrections necessary in each U-103 test.

The maximum retained gas fraction, as well as the mechanisms of gas retention and release, is related to the waste strength. Neglecting the potentially anomalous U-103 upper-tank composite result, the maximum retained gas fractions of the SST waste samples ranged from 0.4 to 0.5. These values are comparable to the maximum retention (0.4 gas fraction) previously determined for bentonite clays of 30-70 Pa shear strength. The relatively small variation in the maximum gas fractions of SST samples of apparently comparable strength may be due to the impact of another waste property (e.g., surface tension) that is not considered in the simple correlation of maximum retention and waste strength.

Contents

Figures

Tables

1.0 Introduction

The Hanford Site is home to 177 underground waste storage tanks, 149 single-shell tanks (SSTs) and 28 double-shell tanks (DSTs), that contain millions of gallons of radioactive waste resulting from the purification of nuclear materials and related processes. The chemical constituents of many of these tanks continue to react because of the thermal and radiolytic conditions within the wastes (King et al. 1997). Products of these reactions include flammable fuels such as hydrogen, ammonia, and methane and the oxidizer nitrous oxide. In 25 of the waste tanks, including 19 SSTs, these flammable gases are known or suspected to be retained in significant quantities (Hanlon 1995). Because of the potential for gas releases and resulting flammable headspace conditions, these tanks have been placed on the Flammable Gas Watch List (FGWL). Developing an understanding of the mechanisms of gas retention and release in these wastes is a critical component of the effort to understand the flammability hazard and to resolve the safety issue (Johnson et al 1997a, b).

1.1 Purpose, Objectives, and Approach

The ongoing goal of this research is to establish an understanding of the mechanisms of flammable gas retention and release in Hanford tanks through laboratory investigations of actual tank wastes. These results support resolution of the Flammable Gas Safety Issue [Tri-Party Agreement Milestone M-40-00 due September 30, 2001 (Johnson 1997)]. Gas bubble retention information gained in the pursuit of safe storage will, in turn, benefit future waste operations including salt-well pumping, waste transfers, and sluicing/retrieval.

Ideally, gas retention and release tests would encompass all waste tanks and all unique waste types within each tank. This is not only impractical, it is also unnecessary; a detailed understanding of bubble retention and release mechanisms on a representative selection of tanks should provide a foundation sufficient to support closure of the safe storage topic. Previous laboratory studies on simulated and actual wastes established a framework to classify gas bubble retention mechanisms (Gauglitz et al. 1994, 1995, 1996). The behaviors observed in other simulated waste (Walker et al. 1994; Rassat and Gauglitz 1995) and actual waste (Bredt et al. 1995; Bredt and Tingey 1996; Rassat et al. 1997) gas retention studies are captured within this general framework. The previous investigations include four DST wastes (AN-103, AW-101, SY-101, and SY-103) and one SST waste (S-102).[a] Considering the relatively large fraction of SSTs at Hanford and on the FGWL, the experimental study of SST waste gas retention and release was underrepresented. The current gas retention experiments include four samples from three SSTs (A-101, S-106, and U-103).

The specific objective of this work is to investigate gas retention and release in a variety of waste types using established experimental techniques that, as accurately and reasonably as

(a) Hanford tanks are formally designated with the prefix 241-, but tank identification without the prefix is generally accepted; the prefix is used infrequently in this report.

possible, reflect the actual tank conditions. In addition, waste sample shear strengths and densities are measured, because these can influence the mechanism and magnitude of gas retention, depending on the waste configuration. The existing gas retention experimental method uses a relatively small waste sample (~50–75 mL) settled in a transparent vessel in which gas bubbles are nucleated and grown over about a day by applying a vacuum in a controlled manner (Rassat et al. 1997). Retained gas volumes are quantified by following changes in waste height, and retained gas bubbles are observed, providing additional qualitative information on the mechanisms of gas retention. Previously, replicate analyses of nearly identical waste composites using evacuation techniques gave repeatable results (Gauglitz et al. 1996; Rassat et al. 1997). This justifies the use of only a single analysis of a given waste type in the current studies.

Bubble retention and release are scale-dependent physical phenomena, and the gas retention experimental method has some limitations. The primary limitations are tied to the geometry of the sample and the time scale of the test. The relatively short, narrow sample does not properly reflect the load at depth in an actual tank, and the vessel walls in the experimental system have greater influence (e.g., wall interactions observed in DST wastes [Rassat et al. 1997]). The short duration of the test and the method of bubble nucleation minimize the opportunity for diffusive transport of gaseous species and may lead to a more uniform distribution of relatively smaller gas bubbles. In spite of the limitations, valuable information is gained on gas retention mechanisms and the potential magnitude of the flammable gas hazard. The experiments produce values of maximum retained gas fraction. As a result of the experimental limitations noted above, these maximum gas fractions tend to be large (compared with retained gas fractions measured in tanks), and therefore can be considered conservative, worst-case estimates of flammable gas storage capacity in the tanks.

The four SST samples to be tested were selected based on criteria including diversity of waste classification (type); behavior indicating that the waste retains, or has the potential to retain, significant quantities of gas; and sample availability (see Section 2 for a more thorough discussion of selection criteria). While it is important to investigate a variety of wastes to characterize potential new gas retention behavior, it is also valuable to demonstrate consistency in gas retention results. The experimental results either affirm the existing models of gas retention and release mechanisms or demonstrate where modifications to the prevailing models may be necessary.

1.2 Gas Bubble Retention Mechanisms

Gauglitz and coworkers (1994, 1995, 1996) identified gas bubble retention mechanisms of potential importance in Hanford wastes. One of these, bubbles retained by direct attachment to particles (armored bubbles, bubble attachment, and aggregates), is thought to play a relatively insignificant role in the safe storage of tank waste; however, these bubbles may play a more significant role in waste handling conditions that require mixing of the waste (e.g., mitigation of SY-101 and waste retrieval). Interestingly, in gas retention experiments on AN-103 waste samples, significant frothing was observed above the supernatant liquid, and it was speculated

that armored bubbles may have played a role (Rassat et al. 1997). The two predominant mechanisms of bubble retention in typical waste configurations are interstitial liquid-displacing bubbles retained by capillary forces in a coarse particulate material and particle-displacing bubbles retained by the yield strength in a continuum or fine particulate material (Gauglitz et al. 1996; Johnson et al. 1997b). These mechanisms are depicted in Figure 1.1. In a coarse particulate medium, the surface tension and pore throats between the particles result in capillary forces that counter the fingering of bubbles between the waste particles and the tendency of bubbles to rise due to buoyancy. Materials in which bubbles displace particles may be considered a continuum. Here, a bubble experiencing an upward buoyant gravitational force must overcome the strength of the material to rise.

Two dimensionless groups govern a transition between these two primary mechanisms of bubble retention (Gauglitz et al. 1994, 1995, 1996). The development is reproduced here for convenience. The first dimensionless group relates gravitational and surface tension forces,

$$\frac{\text{Gravitational Force}}{\text{Surface Tension Force}} = \frac{\Delta\rho g h D_{particle}}{4\gamma} \qquad (1.1)$$

and the second relates waste strength and surface tension forces:

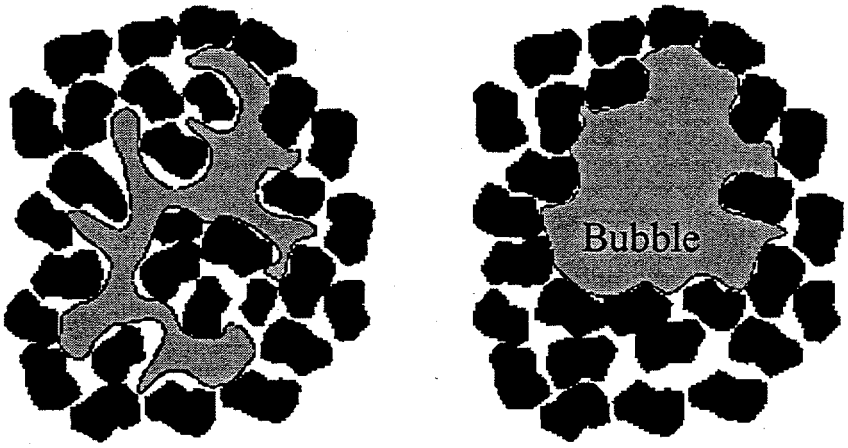

Interstitial-Liquid-Displacing Bubble **Particle-Displacing Bubble**

Figure 1.1. Schematic of a Bubble Fingering Between Particles in a Particulate Material and a Bubble Displacing Particles in a Continuum Material

$$\frac{\text{Strength Force}}{\text{Surface Tension Force}} = \frac{\tau_s D_{particle}}{4\gamma}\left(\frac{A_2}{A_1}\right) \qquad (1.2)$$

In these relationships, γ is the surface tension force, and it reflects the resistance the bubble experiences as it seeks to move between particles. The appropriate length scale is the pore-throat diameter, but here it is represented as the particle diameter, $D_{particle}$, because these two measures are simply related for beds of packed particles (Dullien 1992). In Eq. (1.2), the constant A_2/A_1 is a ratio of areas that resulted from the original analysis (see Gauglitz et al. 1995), and τ_s represents the strength of the material. In Eq. (1.1), $\Delta\rho$ is the density difference between the settled solids and the liquid, g is the gravitational acceleration, and h is the depth below the top of the settled solids. Thus the transition from interstitial liquid-displacing bubbles to particle-displacing bubbles depends not only on waste properties but also on the location of the bubble in the waste column.

Figure 1.2 schematically depicts the two regimes of bubble retention on a single plot. The abscissa of the plot is the ratio of gravitational-to-surface tension forces given by Eq. (1.1), and the right-hand ordinate is the strength-to-surface tension relationship given by Eq. (1.2). The solid curve in the figure defines the transition of interstitial liquid-displacing (dendritic) bubbles retained by capillary forces and particle-displacing bubbles retained by the strength of the material. To date in our laboratory, interstitial liquid-displacing bubbles have been observed only in simulated wastes composed of sands (Gauglitz et al. 1994) and glass or polymethyl-methacrylate (PMMA) beads of varying diameter (Gauglitz et al. 1995; Rassat and Gauglitz 1995) in water. In these relatively large-particle and high-density difference systems, transitions were observed from interstitial liquid-displacing bubbles deeper in the waste to round, particle-displacing bubbles nearer the liquid surface. In actual waste experiments, including the present work, only particle-displacing bubbles have been observed (Gauglitz et al. 1996; Bredt and Tingey 1996; Rassat et al. 1997). Neither the actual waste properties (i.e., difference in nonconvective layer and interstitial liquid densities; particle size) nor the experimental conditions (shallow waste depth) used in laboratory tests have been conducive for observing interstitial liquid-displacing bubbles.

Actual waste experiments have been conducted on both DST and SST wastes represent-ing a wide variety of waste properties. Waste types have ranged from sludges and other sludge-like fine particulate materials, in which only particle-displacing bubbles are expected, to moderate-grained (~0.1 mm diameter estimated) saltcake wastes (e.g., S-102 saltcake) (Gauglitz et al. 1996). Here we incorporate the typical classification of SST waste types as sludge, saltcake, or super-natant liquid (Hanlon 1997). Sludges (precipitated solids resulting from the addition of sodium hydroxide) (Hanlon 1997) are typically fine-particulate materials often described as clay-like or plastic. Saltcake, resulting from crystallization of salts during the concentration of liquid waste, typically has a more distinguishable particulate or granular character. Despite the range of waste particle sizes investigated experimentally, the primary mechanism of gas retention is the particle-displacing bubble. Thus, each of these wastes demonstrates properties of a continuum material.

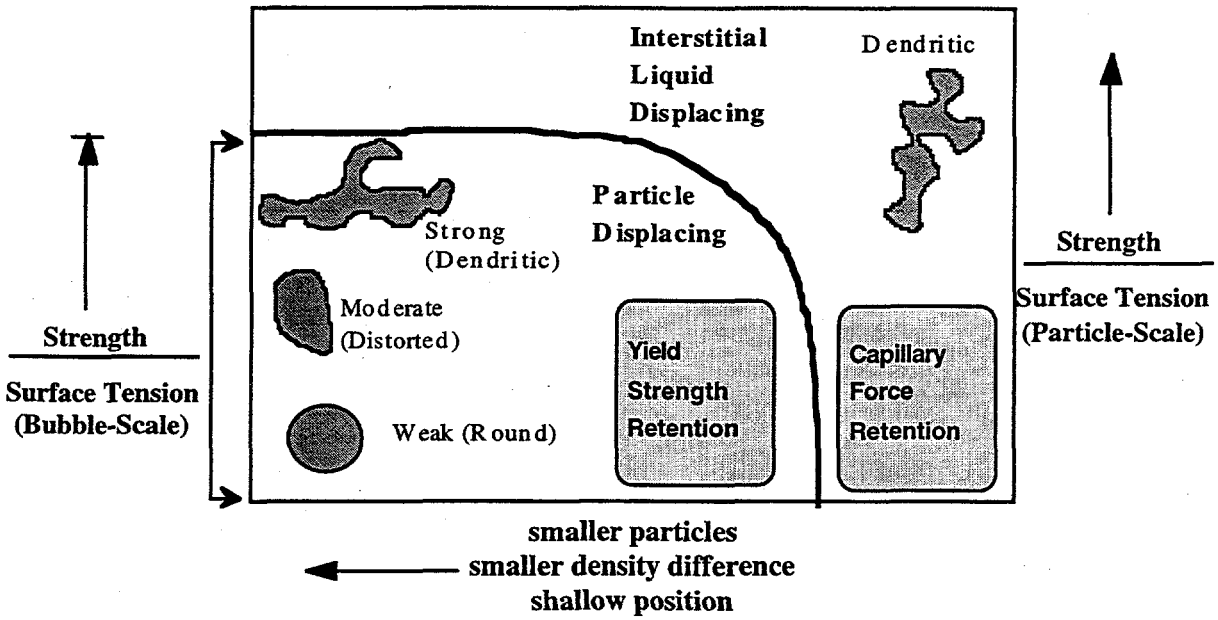

Figure 1.2. Plot of the Predominant Bubble Retention Regimes Resulting from Dimensional Analysis

In a continuum material, the shape characteristics of a retained particle-displacing bubble are affected by the strength of the medium, the size of the bubble, D_{bubble}, and the surface tension force. This is captured in a third dimensionless quantity (Gauglitz et al. 1996):

$$\frac{\text{Strength Force}}{\text{Surface Tension Force}} = \frac{\tau_s D_{bubble}}{\gamma} \tag{1.3}$$

Here, surface tension works to keep the bubble round in the face of the material strength, which seeks to prevent bubble expansion and may lead to distortion of the bubble shape (through a path of least resistance). Thus the bubble diameter, rather than the pore diameter, is the appropriate length scale. The effect of variation in the ratio of strength and surface tension forces (bubble length scale) is shown in Figure 1.2. Equation (1.3) is plotted on the left-hand ordinate, and the change in bubble shape from round in relatively weak materials to a highly distorted dendritic entity in strong materials is shown pictorially.

Although it is expected that both the tensile and shear strengths are important in the growth of bubbles, these two measures of strength are commonly related (see Gauglitz et al. 1995 for a discussion of tensile and shear strength measurements). The shear strength (τ_s) is used in the development above because it is the most easily measured and commonly reported measure of material strength. The strength of a waste material is known to affect the mechanisms of both gas

retention and gas release (Gauglitz et al. 1996; Stewart et al. 1996), and this is summarized in Section 5 for simulated and actual SST waste experimental results.

Section 2 discusses the SST actual waste samples used in gas retention and shear strength tests. The shear strength experimental method and results are described in Section 3, and gas retention measurements are detailed in Section 4. Section 5 is a summary of SST gas retention test results, incorporating results from previous studies. Section 6 contains the references cited, and Appendix A contains a tabulation of gas retention data obtained from the four SST waste samples.

2.0 Actual Waste Samples

The gas retention and shear strength tests described in this report were conducted using samples from SSTs A-101, S-106, and U-103. We determined that these actual waste samples could provide valuable data to broaden our understanding of gas bubble retention and release as it relates to the flammable gas issues. Emphasis was placed on SSTs because previous gas retention studies had investigated bubble retention in only one other SST, S-102, while several DSTs have been studied, including SY-103, SY-101, AW-101, and AN-103 (Rassat et al. 1997; Gauglitz et al. 1996; Bredt and Tingey 1996; Bredt et al. 1995). Several other factors, including sample availability, were also considered when choosing the samples for gas bubble retention and release studies; these factors are presented in Table 2.1. Tank S-102, the SST previously tested, is also included in the table for comparison.

The gas retention sample selection criteria in Table 2.1 may be broadly categorized in terms of Flammable Gas program- and gas retention task-specific considerations. From a programmatic viewpoint, tanks selected for bubble retention studies provide a more complete picture of all flammable gas issues. Criteria include having tanks on both the Flammable Gas (fg) or Organic (org) Watch Lists to get maximum information return on investment and having complementary information from in-tank retained gas sampler (RGS) gas fraction measurements and gas generation-rate studies. From a gas-retention, task-specific perspective, a primary driver is developing a complete understanding of gas-bubble retention and release mechanisms in all characteristic tank wastes. The wastes are categorized by type (e.g., double-shell slurry feed [DSSF] or noncomplexed [NCPLX]), cluster, and configuration. Waste cluster and configuration designations are based on factors such as particle size, liquid content, layering, or other physical characteristics that may affect gas retention. Four distinct waste configurations have been defined that encompass nine waste clusters of 54 watch-list SSTs (Stewart et al. 1996; Agnew 1995; Remund et al. 1995). The SST samples used in gas retention testing shown in Table 2.1 represent three of four waste configurations and three of nine clusters. Table 2.1 also includes any additional items considered in choosing these tanks for gas retention testing. For example, two separate samples from Tank U-103 (an upper-tank sample and a middle-tank sample) were tested because RGS measurements in the upper-tank segments (1–3) showed significantly more retained gas than in the lower-tank segments (4–10) (Mahoney et al. 1997).

Table 2.2 summarizes the actual tank waste samples tested. Additional details of tank histories and status are presented in the sections that follow. Samples from Tank A-101 were collected during the Core 154 and 156 sampling events between July 11 and July 25, 1996, and were delivered to PNNL's 325-A High-Level Radiochemistry Facility (HLRF) on November 18, 1997. The A-101 gas retention sample (ID S97M000176) was spent RGS material. Samples from Tank S-106 were collected during the Core 183 and 184 sampling events between February 12 and March 17, 1997, and were delivered to PNNL's 325-A HLRF on June 18, 1997. Of the three distinct samples of S-106 available (Table 2.2), only a single sample from S-106 (ID S97T000383) was used in gas retention testing because only one sample was needed to

Table 2.1. Waste Sample Selection Basis

Tank	Waste Type	Waste Cluster	Waste Config	Watch List	RGS Testing	Gas Generation Testing	Additional Comments
A-101	DSSF	22	1B	fg/org[a]	Completed	Complete in FY 1998	Waste is in an unexpected configuration, with the nonconvective layer on top of the convective layer.
S-102	DSSF	13	1A	fg/org	Complete in CY 1998[b]	Completed	Gas retention and release studies were completed in FY 1996.
S-106	NCPLX	20	2A	none	Completed	Complete in FY 1998	Barometric pressure evaluation (dL/dP) showed high gas retention (15–19%), while the majority of RGS measurements showed a maximum of 10%.
U-103	NCPLX	13	1A	fg/org	Completed	Complete in FY 1999	RGS measurements showed ~10% retained gas in lower segments while the upper segments indicated ~40%.

(a) fg = flammable gas watch list; org = organic watch list.
(b) CY = calendar year.

Table 2.2. Samples Used in Gas Retention and Shear Strength Experiments

Tank	222-S ID	Jar #	Tank Riser	Core	Segment	Location Within Segment
A-101	S97M000176	S97M000176	15	154	5	NA
A-101	S97M000213	S97M000213	24	156	16	drainable liquid
S-106	S97T000383	11830	8	183	8	lower half
S-106	S97T000385	11894	8	183	9	lower half
S-106	S97T000386	11825	7	184	4	upper half
U-103 (upper)	S97M000224 (composite of four jars)	11878	13	182	1	upper half
		11876		182	1	lower half
		11885		182	2	upper half
		11884		182	2	lower half
U-103 (middle)	S97M000229 (composite of four jars)	12185	13	182	5	upper half
		12198		182	5	lower half
		12199		182	6	upper half
		12195		182	6	lower half

(a) 222-S is a laboratory on the Hanford Site.

complete the set of four scheduled to be tested in FY 1998. However, all three S-106 samples were tested for shear strength. Samples from U-103 were collected during the Core 182 sampling event between April 2 and April 8, 1997. Two composite U-103 samples were prepared at the 222-S Laboratory between November 5 and 10, 1997, and these were delivered to PNNL's 325-A HLRF on November 20, 1997. Experiments were conducted on both U-103 composites. Sections 2.1, 2.2, and 2.3 describe each tank configuration and sampling history in more detail.

2.1 Tank A-101

Tank A-101 is an SST located in the Hanford 200 East Area. The tank has an operating capacity of 3,785 kL (1,000 kgal) and contains about 3,600 kL (953 kgal) of waste: 11 kL (3 kgal) of sludge and 3,596 kL (950 kgal) of saltcake with a total waste height of 922 cm (363 in.) (Hanlon 1998). The waste is made up of two distinct layers: a lower, convective layer described as a salt slurry and an upper, nonconvective layer described as a moist salt (Shekarriz et al. 1997), which, as previously indicated, is an inverted and unexpected configuration. This tank is currently on both the Flammable Gas and Organic Watch Lists. Tank A-101 was put into active service in January 1956. Its detailed fill history has been compiled in the A-101 Tank Characterization Report (Field et al. 1997). Between 1956 and 1973, the tank was filled with a combination of PUREX (plutonium-uranium extraction) high-level waste (HLW) and organic wash wastes (OWW). Most of this waste was transferred to other A-Farm and C-Farm tanks during this same period. Between 1973 and 1975, A-101 received strontium recovery supernatant liquid (SRR) from B Plant and supernatant liquid from the sluicing of other HLW tanks in the A and AX Tank Farms. By 1976, all but 11 kL (3 kgal) of sludge was transferred to Tanks A-106 and C-104. From 1976 to 1980, Tank A-101 was filled with dilute DSSF from evaporator campaigns 80-10 and 81-1. Partial isolation of Tank A-101 was completed in 1982, but the tank remains to be stabilized (Brevick et al. 1996).

Vapor samples were taken from Tank A-101 in June 1995, solid/liquid grab samples in April 1996, and push core samples in July 1996. The core samples collected in 1996 were used in the testing reported in this document. Two cores of 19 segments each were recovered from the tank during the July 1996 sampling event; Core 154, riser 15 was sampled from July 11 to 18, 1996, and Core 156, riser 24 samples were obtained from July 22 to 25, 1996. Drainable liquid made up most of the sample for segments 11 through 19 for both cores and segment 10 of Core 156. Segments 1 through 9 of both cores contained solids classified as moist salt and had no drainable liquid.

Figure 2.1 presents the temperature and gas fraction profiles for Tank A-101. The temperature within the waste is monitored using a single thermocouple tree containing 18 thermocouple probes. The temperatures presented in Figure 2.1 represent the average temperatures between October 1996 and October 1997.[a] The waste in A-101 has a total height of 922 cm. The

(a) Temperature data were downloaded via the TWINS2 Interface from the SACS database (Glasscock 1993) on October 28, 1997.

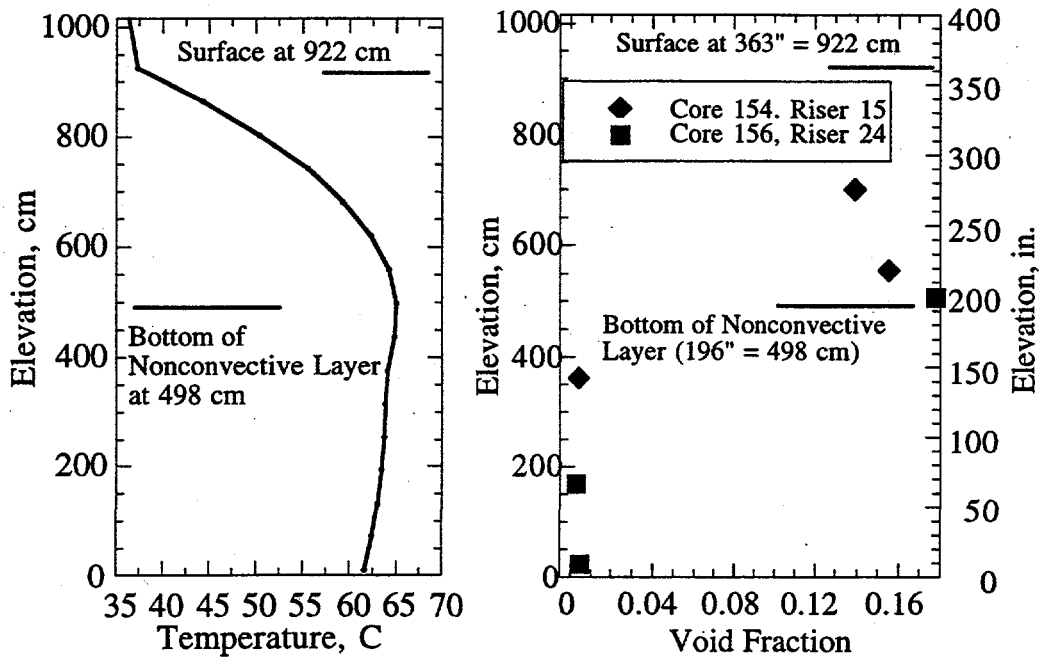

Figure 2.1. Temperature and Gas Fraction Profiles in Tank A-101

temperature profile shows a thermally convective layer extending from the bottom of the tank to a height of 498 cm with a thermally nonconvective layer above. This layering model is consistent with the observations of the sample extrusions, classifying the upper material as moist salt or wet salt and the lower layer as salt slurry or liquid. The convective layer had an average yearly temperature range of 61 to 65°C (142 to 149°F), while nonconvective layer average temperatures ranged from 37 to 64°C (99 to 147°F). The solid sample used in these tests came from segment 5 of Core 154, which originated from between approximately 675 and 723 cm above the tank center bottom. The same sample was used in RGS testing (Shekarriz et al. 1997). Based on the average temperature profile and the need to select one representative tank temperature, gas retention testing was conducted at a temperature of approximately 53°C (127°F).

The A-101 gas fraction profile in Figure 2.1 is reproduced from Shekarriz et al. (1997, Figure 4.11). The RGS data also show that two distinct layers exist in this tank. Below 500 cm, in the convective liquid, there is essentially no gas bubble retention. Above 500 cm, in the nonconvective solids, gas is retained with a maximum gas fraction of approximately 18% at the bottom of the nonconvective layer.

2.2 Tank S-106

Tank S-106 is an SST in the Hanford 200 West Area. The tank has an operating capacity of 2,870 kL (758 kgal) and contains an estimated 1,813 kL (479 kgal) of NCPLX waste: 15 kL (4 kgal) of supernatant liquid, 1,692 kL (447 kgal) of saltcake, and 106 kL (28 kgal) of sludge (Hanlon 1998). Authors of the Tank Characterization Report for Tank S-106 (Field et al. 1998) report different volumes of liquid and solid waste present in the tank than are reported in Hanlon (1998). Field et al. estimate a larger supernatant volume, 201 kL (53 kgal), and a smaller solid waste volume, 1,612 kL (426 kgal). A gradual increase in the surface level of the waste has been noted since 1989, from approximately 442 cm (173 in.) in January of 1989 to about 464 cm (182.5 in.) in June of 1998.[a] In addition, tank samples and surface-level measurements indicate that the waste level in the tank is not uniform. Tank S-106 is out of service, as are all SSTs, and is categorized as sound. The tank is not on any watch list.

A detailed fill history for Tank S-106 has been compiled in the S-106 Tank Characterization Report (Field et al. 1998). From the second to third quarters of 1953, Tank S-106 was filled with waste from the reduction-oxidation (REDOX) facility. REDOX cladding waste (CWR) was transferred from S-106 to Tank S-103 in 1955. From 1973 to 1975, S-106 received evaporator bottoms waste from the 242-S Evaporator via Tank S-102. The tank was removed from service in 1976 and was partially isolated in 1982. A jet pump was installed and activated in the fourth quarter of 1983. From 1983 to 1984, 378 kL (99.8 kgal) of liquid was pumped from Tank S-106, and the tank has since been declared interim stabilized (Swaney 1996).

Solid/liquid grab samples were taken from Tank S-106 in June 1975 and January 1992; vapor samples were taken in June 1996; and three push-mode core samples were taken in February and March of 1997. The first push-mode core sample, Core 183, consisted of ten segments removed from riser 8 between February 12 and February 21, 1997. The segment 2 sample was designated for RGS sampling but was discarded because the valve was leaking when the sampler was being prepared for the extrusion. Ten push-mode core segments were scheduled to be removed from Tank S-106, riser 7 during Core 184, but because of problems encountered during sampling, only six segments were obtained. The sampler was unable to penetrate beyond the sixth segment due either to an obstruction or to the strength of the material (Field et al. 1998; Mahoney et al. 1997). The Core 184 segments were collected between February 24, 1997 and March 17, 1997. Because two full cores were not obtained from the first two risers, a third push-mode core sample, Core 187, was scheduled for removal from Tank S-106, riser 14. Additional sampling problems were encountered, and only three segments (of the scheduled 13) were obtained between March 19 and March 21, 1997. Results from these core samples suggest the waste in S-106 consists of two distinct layers: an upper liquid layer ranging from 40 to 200 cm (16 to 79 in.) in thickness and a lower, high-solids, saltcake layer ranging from 260 to 420 cm (102 to 165 in.) in thickness. There is also a thick, dry crust around the perimeter of the tank. The waste properties are not consistent among the risers, suggesting that the waste is not laterally uniform in the tank.

(a) Surface level data were downloaded via the TWINS2 Interface from the SACS database (Glasscock 1993) on June 3, 1998.

Figure 2.2 presents the temperature and gas fraction profiles for Tank S-106. The temperature within the waste is monitored using a single thermocouple tree in riser 2 containing 14 thermocouple probes. The temperatures presented in Figure 2.2 represent the average temperatures between October 1996 and October 1997.[a] During this time, the waste in S-106 had a total height of 457 to 461 cm (180 to 181.5 in.).[b] The temperature profile shows the parabolic shape characteristic of conductive heat transfer with generation. No significant convective layer, which would appear as a uniform temperature, is indicated. The average nonconvective layer temperatures range from ~21 to 26°C (70 to 79°F). The sample used in the gas retention tests came from segment 8 of Core 183, which originated from an elevation between approximately 97 and 145 cm above the tank center bottom. Based on the average temperature profile and the need to select one representative tank temperature, gas retention testing was conducted at the ambient cell temperature of 26 to 30°C (79 to 86°F). In addition, due to apparatus limitations, only one temperature-controlled sample is possible at a time, and the need for an elevated temperature in the A-101 sample was of higher priority.

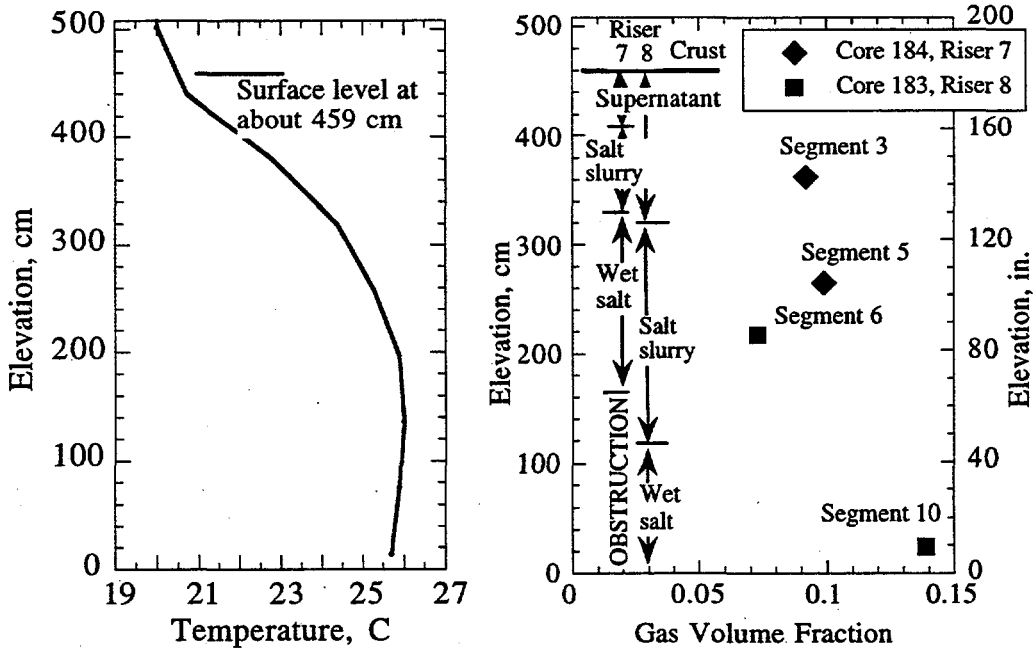

Figure 2.2. Temperature and Gas Fraction Profiles in Tank S-106

(a) Temperature data were downloaded via the TWINS2 Interface from the SACS database (Glasscock 1993) on October 28, 1997.
(b) Level data were downloaded via the TWINS2 Interface from the SACS database (Glasscock 1993) on June 4, 1997.

The S-106 gas fraction profile in Figure 2.2 is reproduced from Mahoney et al. (1997, Figure 4.2.5). The retained gas sampler was used in risers 7 and 8 to sample four segments, two from each riser. The in situ gas volume fraction ranged between 7.3 and 14%.

2.3 Tank U-103

Tank U-103 is an SST located in the Hanford 200 West Area. The tank has an operating capacity of 2,010 kL (530 kgal) and presently contains an estimated 1,771 kL (468 kgal) of NCPLX waste: 49 kL (13 kgal) of supernatant, 458 kL (121 kgal) of salt slurry, 1,143 kL (302 kgal) of saltcake, and 121 kL (32 kgal) of sludge (Hanlon 1998). Tank U-103 is on the Flammable Gas and Organic Watch Lists.

Tank U-103 entered into service in February 1947. A detailed fill history has been compiled in the preliminary U-103 Tank Characterization Report (Kupfer et al. 1997). Tank U-103 received metal waste from the first quarter of 1947 until the fourth quarter of 1956. During 1955, waste was removed for the uranium recovery process, and in the fourth quarter of 1956 the heel was sluiced. The tank received REDOX waste from the first quarter of 1957 until the second quarter of 1975. From the third quarter of 1975 to the fourth quarter of 1977, U-103 received transfers of evaporator feed and other wastes from various tanks. The final waste transfer was nitric acid/potassium permanganate ($HNO_3/KMnO_4$, partial neutralization feed) waste from evaporator operations in the fourth quarter of 1977. This addition aided in creating saltcake from the evaporator operations. Tank U-103, which was labeled inactive in 1978, is passively ventilated, has been partially isolated, and is awaiting interim stabilization (Brevick et al. 1994).

Vapor samples were taken from Tank U-103 in February 1995; solid/liquid grab sampling was completed in May 1995; and push-mode sampling was done in risers 2, 7, and 13 in October 1996, January 1997, and April 1997, respectively. Only two segments were removed during the October 1996 push-mode sampling in riser 2, Core 175 because the waste (or some object imbedded in it) proved impenetrable. Core 176 consisted of nine segments removed from riser 7 on January 21 and 22, 1997. Core 182, which is used in the testing reported here, consisted of ten segments removed from riser 13 between April 2 and April 8, 1997. Results from the core samples in risers 2, 7, and 13 suggest that Tank U-103 waste is not laterally uniform. The thickness of the top layer of liquid varied over the three risers, and sludge slurry was present at the top of riser 13, but not the others (Mahoney et al. 1997). Moist saltcake was present in the bottom segments of risers 7 and 13 (bottom segments were not obtained in riser 2).

Figure 2.3 presents the temperature and gas fraction profiles for Tank U-103. The temperature within the waste is monitored with a single thermocouple tree in riser 1 containing 11 thermocouple probes. The temperatures presented in Figure 2.2 represent the average between October 1996 and October 1997.[a] The waste in Tank U-103 has a total height of approximately

(a) Temperature data were downloaded via the TWINS2 Interface from the SACS database (Glasscock 1993) on October 28, 1997.

455 cm. The temperature profile shows the parabolic shape characteristic of conductive heat transfer with generation. No significant convective layer, which would appear as a uniform temperature, is indicated. However, the temperature profile at this riser may not be representative of most of the waste because the riser is so close to the tank wall (Mahoney et al. 1997). The average nonconvective layer temperatures range from ~24 to 29.5°C (75 to 85°F). The U-103 upper-tank samples used in the gas retention tests came from segments 1 and 2 of Core 182, which originated from an elevation approximately 394 to 447 cm above the tank center bottom. The U-103 middle-tank samples used in the gas retention tests came from segments 5 and 6 of Core 182, which originated approximately 200 to 297 cm above the tank center bottom. Based on the average temperature profile and the need to select one representative tank temperature, gas retention testing for both the upper and middle-tank segments was conducted at the ambient cell temperature of 26 to 30°C (79 to 86°F).

The U-103 gas fraction profile in Figure 2.3 is reproduced from Mahoney et al. (1997, Figure 4.1.5). The in situ gas volume fraction for segment 2 of Core 176, riser 7 was about 44%; the in situ gas volume fractions for the lower segments of Core 176, riser 7 were much lower, at an average of 9.5%. As a result of this large difference in measured gas volume fraction, gas retention tests were conducted on samples from both upper and middle segments of Tank U-103.

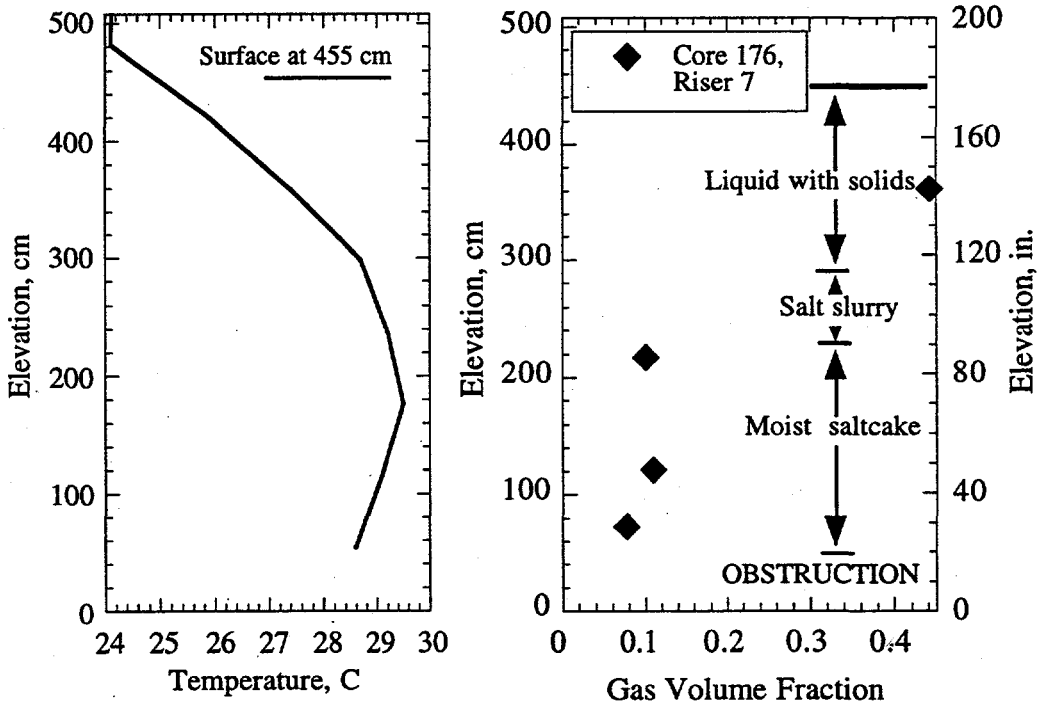

Figure 2.3. Temperature and Gas Fraction Profiles in Tank U-103

3.0 Sample Shear Strengths

The capacity of SST wastes to retain gas is a function of the waste strength (see Section 5), and for the relatively small gas retention samples available (~100 g), shear strength is the appropriate laboratory measurement. The experimental section describes the instrumentation and technique used to measure the shear strengths of waste samples. The shear strength results for six waste samples from Tanks A-101, U-103, and S-106 are discussed in Section 3.2.

3.1 Experimental

The shear strengths of waste samples were determined using a Haake model M5 measuring head electronically remoted for in-cell operation in the 325A HLRF and following an established procedure.[a] All samples were analyzed at least twice, and, depending on sample size, some were analyzed up to four times. Samples from Tanks U-103 and S-106 were analyzed at ambient hot cell temperature, between 27 and 28°C. The sample from Tank A-101 was placed in an oven at 55°C for approximately 48 hours; the sample was then analyzed twice within 15 minutes of its removal from the oven.

Shear strength is a measure of the force required to cause shear failure along a cylindrical surface created by the shear vane in a soft solid material (Nguyen and Boger 1992). Since this property is dependent upon sample history, the shear strength was measured on the samples in the original jars shipped to PNNL before any mixing and after the samples were left undisturbed for a minimum of two weeks. The PNNL-manufactured shear vane with the dimensions H_v = 1.582 cm (height) and D_v = 0.800 cm (diameter) was placed in the sample and rotated at a rate of 0.6 rpm. The stress required to maintain the rotational speed was recorded as a function of time. The shear strength, τ_s, was then calculated according to Eq. (3.1), where 4.9×10^5 is the maximum torque of the M5 head, $\%\tau/100$ is the fraction of the total torque which was set as full scale on the plot of the shear stress, and S_τ is the fraction of full scale recorded on the plot. For example, if the full scale on the plot was set to 25% and the shear strength was measured at 15% on the plot, then the total torque (the numerator of Equation 3.1) would be [(25/100) x 0.15 x 4.90 x 10^5] dyne•cm. Shear strength in the SI unit of Pascals (Pa; N/m^2), and as reported here, is a factor of 10 less than the alternative unit, $dyne/cm^2$.

$$\tau_s = \frac{4.90 \times 10^5 \frac{\%\tau}{100} S_\tau}{\frac{\pi H_v D_v^2}{2} + \frac{\pi D_v^3}{6}} \qquad (3.1)$$

(a) PNNL Technical Procedure PNL-ALO-501, "Laboratory Procedure for Measurement of Physical and Rheological Properties of Solutions, Slurries, and Sludges."

Before we conducted the shear strength analyses, we performed an instrument calibration check with the Haake model MV1 viscometer geometry and a 96.5 cP (at 25°C) viscosity standard purchased from Brookfield.[a] The standard measured 90.3 cP at a shear rate of 351 s^{-1} at the cell temperature of 28°C; the expected reading at this slightly elevated temperature was 93.3 cP. The difference in measured and expected values was well within the acceptable range of ±10% error, indicating proper torque measurement. After the shear strength measurements were complete, we conducted a post-experimental instrument performance check by submerging the shear vane 3.0 cm into a high-viscosity standard (Brookfield, 99,200 cP at 25°C)[a] and rotating it at 0.6 rpm. The measured torque for this standard was within 8% of the expected value at the cell temperature. The expected error in the accuracy of a single shear strength measurement is about ±10% of the measured value. Because of actual waste sample inhomogeneities, the precision of repeated shear strength measurements at different locations within the sample is typically much less.

3.2 Shear Strength Results

Selected samples from Tanks A-101, S-106, and U-106 were analyzed for shear strength. Results from these analyses, including average shear strengths, the number of replicate shear tests per sample, and the variability in the measurements, are listed in Table 3.1. The shear history of the samples is also tabulated because the shear strength of a material can depend on previous handling. With the exception of the shear induced during the tank core sampling and sampler extrusion process, the samples identified as "undisturbed" have no significant shear history. The three samples from S-106 are categorized as undisturbed. The sample from Tank A-101 is spent RGS material. The RGS system stirred the sample at less than 1 rpm for about one-half hour using a bladed impeller to release trapped gas (Shekarriz et al. 1997). This mixing would be expected to decrease the measured shear strength of thixotropic waste. The first sample from Tank U-103 was a composite of material from segments 1 and 2 of Core 182; the second was a composite from segments 5 and 6 in the same core. The composites were prepared in the 222-S Laboratory prior to delivery to PNNL by combining material from the segments and homogenizing. The shear forces applied to the samples during homogenization were not reported. For most tank materials, the measured shear strength decreases after a sample has been mixed.[b]

The most surprising result is the high 16,000 Pa shear strength of the segment 4 upper-half S-106 sample, which is about an order of magnitude stronger than the samples lower in the tank (1,100 Pa for segment 8 lower half and 1,800 Pa for segment 9 lower half). Following shear strength analysis, hot cell personnel tried to stir the material from the upper half of segment 4 and confirmed qualitatively the high stiffness. X-ray analysis of the segment 4 upper-half sample conducted during the core sampling indicated a sample structure consisting of wet salt and

---

(a) Brookfield viscosity standards were obtained with certificates of calibration from Brookfield Engineering Laboratories, Inc.

(b) Bredt PR, JD Hudson, and JM Tingey. 1995. *Effects of Dilution on the Physical and Chemical Properties of Tank 241-SY-103 Waste.* Letter Report PNL MIT 092995, Pacific Northwest Laboratory, Richland, Washington.

Table 3.1. Shear Strengths for Samples from Tanks A-101, S-106, and U-103

Tank	Core	Segment	Shear History	Sample Temp, °C	Avg. Shear Strength, Pa	No. of Replicates	% Relative Deviation[a]
A-101	154	5	Mixed	55	640	2	28
S-106	184	Upper Half of 4	Undisturbed	27	16,000	3	56
S-106	183	Lower Half of 8	Undisturbed	27	1,100	4	38
S-106	183	Lower Half of 9	Undisturbed	28	1,800	3	23
U-103	182	1 and 2	Mixed	28	750	2	14
U-103	182	5 and 6	Mixed	28	4,500	2	23

(a) Calculated as relative percent difference for two replicates or determined from the standard deviation for three or four replicates.

some large crystals (Mahoney et al. 1997). It is likely that the exceptional strength of this sample results from its crystalline nature. It is also possible that, in the half-year storage in the 325A HLRF, the sample partially dissolved and recrystallized in accord with temperature swings in the facility from the summer (~35–38°C) to winter (~28°C). Note that while these S-106 samples are taken from different elevations within the tank, they represent different cores as well. The samples from segments 8 and 9 are from Core 183, and the sample from segment 4 originated from Core 184. During Core 184 sampling, the sampler was unable to penetrate beyond the sixth segment due either to an obstruction or to the strength of the material (Field et al. 1998; Mahoney et al. 1997). Although this does not provide direct evidence for the high measured shear strength of the segment 4 sample, it is consistent. It is unclear whether differences in the S-106 sample shear strengths are due to lateral inhomogeneities, vertical variations, or both. The segment 8 lower-half S-106 sample was selected for gas retention testing.

For U-103 samples, the composite of segment 5 and 6 materials was considerably stronger (4,500 Pa) than the 750 Pa determined for the higher elevation segments (1 and 2) composite. Because both these composites were prepared at the 222-S Laboratory approximately two months before testing, the differences in shear strength appear to reflect variations in waste properties rather than differences in shear history. The A-101 sample of spent RGS material had a moderate strength of 640 Pa even though it was sheared for RGS testing; and the A-101 shear strength test temperature of 55°C was ~27°C higher than the other samples. As noted above, lower temperatures may lead to more crystallization and higher shear strengths in a sample. Efforts were made to conduct the shear strength measurements near the reported tank temperatures for all three tanks (see Section 2).

As presented in Sections 4 and 5, the retained bubble shapes and gas release characteristics of bubble-laden A-101, S-106, and U-103 composites in the gas retention vessels were consistent with the behavior of bentonite clay simulated wastes having shear strengths on the order of 50 Pa. These apparent strengths are much lower than the shear strengths presented in Table 3.1,

which range from 750 Pa to 4,500 Pa on the as-received U-103 composite samples and are 640 Pa and 1,100 Pa on the as-received A-101 and S-106 samples, respectively. These discrepancies are likely due to shearing of the sample in the vessel loading process and the limitations in the method used to estimate waste strengths of the in situ gas retention samples (see Section 5). Previous investigations showed that the shear strengths of freshly composited AW-101 tank waste samples (<300 Pa, the detection limit for the apparatus described in Section 3.1) were less than the minimally disturbed subsamples (up to 2100 Pa) tested prior to compositing (Rassat et al. 1997).

Other measures of tank waste strength exist. The in-tank ball rheometer method has produced yield stress results for several DSTs (Meyer et al. 1997). Rassat et al. (1997) compared the ball rheometer yield stress values for AW-101 and AN-103 tank wastes to shear strength measurements, and the average yield stress values were up to an order of magnitude lower than laboratory measured shear strengths. Shear strength and yield stress are fundamentally different properties of the materials, and the two measures of strength are not expected to be the same, although they may be related. For the SST wastes of current interest, ball rheometer data are not available. Gauglitz and Aikin (1997) reviewed horizontal extrusion data for several DST and SST tank wastes and used horizontal extrusion data from simulated wastes as calibration standards to estimate actual waste shear strengths. The estimated strengths for AW-101 and AN-103 using the extrusion technique were, in general, considerably lower than the shear strength measurements for tank samples reported by Rassat et al. (1997), but they agreed reasonably well with the ball rheometer results. The extrusion method has not yet been applied to estimate the strengths of A-101, S-106, and U-103 wastes.

4.0 Gas Retention Measurements

This section describes gas retention experiments conducted on samples from SSTs A-101, S-106, and U-103. Section 4.1 describes the apparatus, approach, and methods applied in the gas retention experiments. Sections 4.2, 4.3, and 4.4 present both the qualitative visual evidence of gas bubble retention and release mechanisms and the respective quantitative results for these tanks. Section 4.5 summarizes and compares the gas retention data for the three tanks.

4.1 Experimental

The evolution of the gas retention apparatus for simulated and actual waste experiments is described in previous work (Rassat and Gauglitz 1995; Bredt et al. 1995; Bredt and Tingey 1996; Gauglitz et al. 1996; Rassat et al. 1997). The experimental system described in Rassat et al. (1997), including the retention vessels, electronic pressure control system, and video system, was used in this study with only minor modifications. A more detailed description of the apparatus and methods is given in the previous report, and the information is summarized below for convenience.

One deviation to be noted is that in the present experiments, the waste samples were not irradiated with a cesium gamma source prior to evacuation, a method typically used to generate a small initial gas volume within the sample. It was predicted, and shown experimentally, that, even without pre-irradiation, enough gas was present in the samples to attain maximum retention using only the vacuum system.

4.1.1 Vessels and Samples

The retention vessels are constructed from nominally 2.54 cm (1 in.) inside diameter (i.d.) by 3.18 cm (1.25 in.) outside diameter (o.d.) acrylic tubes that are graduated every 0.5 cm along their 25-cm length. The machine-etched heights (in mm) marking each centimeter along the length of the vessels were painted with a reflective-paint pen to improve readability. Each vessel was calibrated for volume as a function of height using a water addition method in order to determine waste sample volumes from observed waste levels (heights) during the gas retention experiments. The average height-specific volume of the vessels is 4.93–4.97 mL/cm. Additionally, four replicate calibrations to 10.0-cm and 20.0-cm heights were conducted on a single vessel. The uncertainties in the repeated measurements determined from the standard deviations in added water volumes (mass x density) were less than ±0.004 mL/cm for both levels. All masses measured during vessel calibration and vessel loading and density measurements were obtained from calibrated balances accurate to the nearest 0.02 g or better.

The as-received waste samples were mixed gently by hand to aid in their transfer to the retention vessel by pouring. In the case of A-101, a small amount (~6% by weight of the *total* sample) of supernatant liquid from the same tank was mixed into the sample to thin it for transfer. In all cases, the retention vessels were approximately half filled, and the amount of sample transferred to the vessel was weighed. The samples were allowed to settle for a minimum of two weeks and up to four weeks. Just before sample evacuation, the bulk of any freestanding liquid was removed from the SST waste samples, using a plastic transfer pipette, and weighed. The density of this liquid was determined by measuring the volume and mass of liquid placed in a 10±0.1-mL graduated cylinder following a standard procedure.[(a)] Only enough liquid was available for a single analysis. Therefore, reported uncertainties in the liquid density are propagated from the estimated uncertainties of the mass (±0.02 g) and volume (±0.1 mL) measurements. The residual freestanding liquid in the retention vessel at the start of an evacuation was small (<0.2 cm height). The supernatant density and volume of residual liquid can be used to estimate the density of the settled solids layer (Rassat et al. 1997). Although density values are not critical for understanding these SST experiments, the results are reported in Section 4.5 for completeness. Uncertainties in the pre-evacuation settled solids densities were determined by propagating estimated uncertainties in sample mass, volume, and liquid density. In all cases, the uncertainty in the settled solids density was less than 0.03 g/ml.

Two samples of U-103 and one of S-106 tank waste were tested at ambient hot cell temperature (~26–30°C). The sample of A-101 was tested at 51–53°C. The elevated temperature was also maintained in the sample-settling phase, except for a few low (ambient) temperature excursions resulting from recirculation pump failure. For temperature control, the vessel was fitted with a sealed acrylic water jacket (5.1 cm x 5.1 cm cross-section and ~30 cm tall). Water was recirculated at approximately 3–4 L/min in a closed loop through a heat exchanger bed, which was heated by a water bath. Calibrated type K thermocouples were placed in the loop at the inlet and outlet of the water-jacketed vessel. All four sample vessels were secured in a steel vessel rack in the 325A HLRF during testing.

4.1.2 Vacuum System and Pressure Control

The vessels are sealed vacuum-tight with O-rings fitted in a stainless steel top. A 1/4-in. (0.64-cm) fitting welded to the top connects a vessel to the vacuum system. The vacuum and pressure control system, as set up in the 325A HLRF, is depicted in Figure 4.1. The key components of the system are the vacuum pump, 1/4 in. (0.64 cm) o.d. stainless steel and rigid plastic tubing, a series of mechanically actuated needle and ball valves, a single electronically controlled valve (0.5 L/min maximum flow rate), two 0–1000-mm-Hg absolute pressure transducers, and the associated readout and control electronics. The secondary pressure

(a) PNNL Technical Procedure PNL-ALO-501, "Laboratory Procedure for Measurement of Physical and Rheological Properties of Solutions, Slurries and Sludges." Section 5, "Procedure for Determination of Vol%, Wt% and Densities of Centrifuge Solids and Supernate," was used.

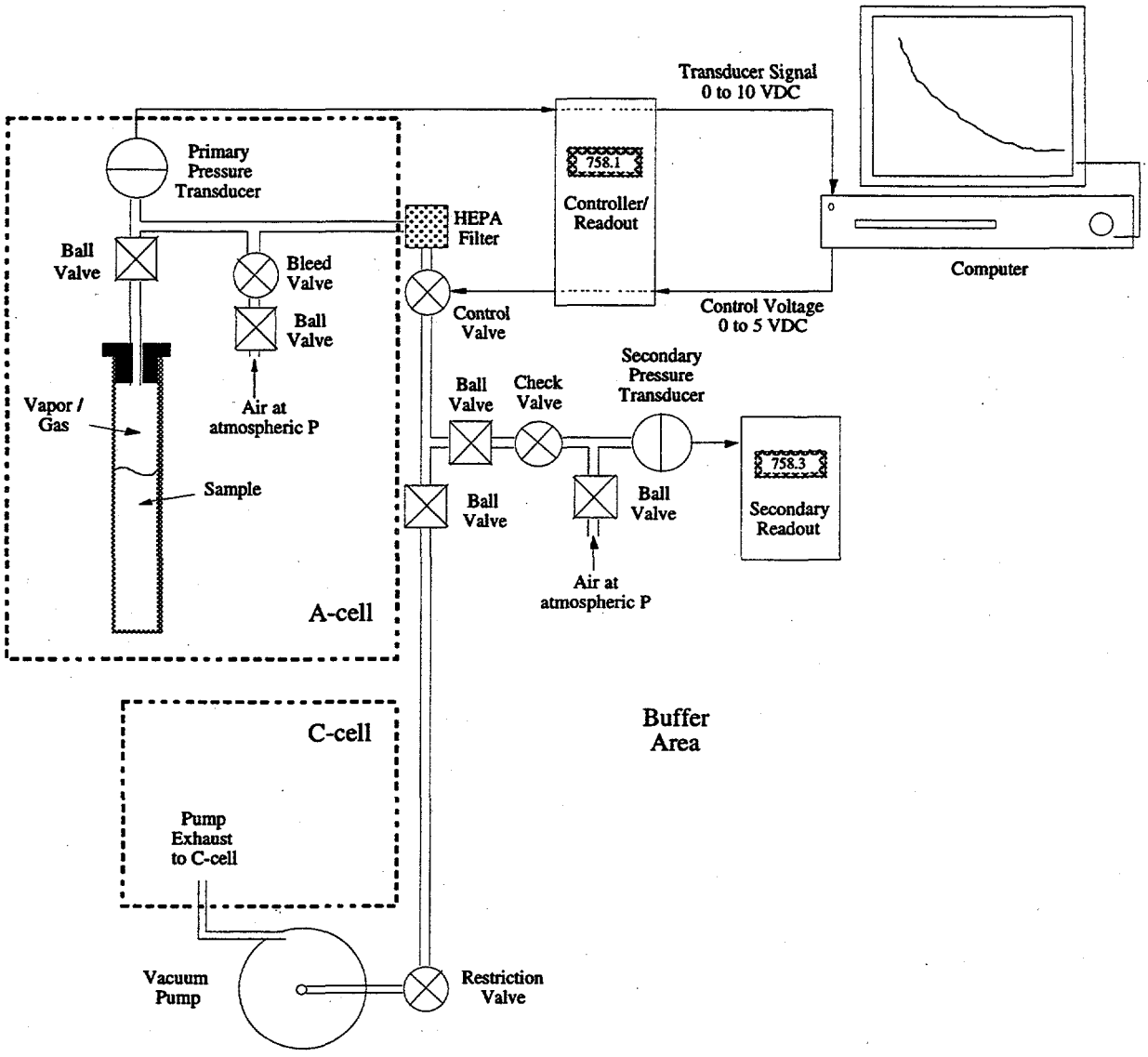

Figure 4.1. Pump and Vacuum Pressure Control System

transducer shown in the figure was externally calibrated (<±0.5% of reading), and it was employed to "user-calibrate" the primary (in-cell) transducer and to perform routine system performance checks.

During a sample evacuation, the system pressure at the primary transducer was regularly and automatically measured, logged to a computer data acquisition system, and compared with the set point pressure. A proportional-integral-derivative (PID) pressure controller actuated the electronic control valve to maintain the measured pressure near the set point. To attain a consistent sample growth rate in the course of an evacuation experiment, the set-point pressure (P_{set}) was adjusted continually using a pressure program given by the following function:

$$P_{set} = P_{init}\left(\frac{1}{1+t/t_{set}}\right) \tag{4.1}$$

where P_{init} is the initial set-point pressure in mm Hg, typically set to 760 mm Hg, t_{set} is the first pressure half-life in minutes, and t is the elapsed time in minutes from the start of the pressure program. The parameter t_{set} was set to allow for approximately one-day experiments. Assuming ideal gas law behavior for the retained gas, the pressure program given by Eq. (4.1) results in a linear sample volume growth in time (Rassat et al. 1997).

4.1.3 Video System

Images of the waste sample were recorded during an evacuation experiment for post-experimental analysis. In any given experiment, two video cameras were operated simultaneously. One camera was positioned to view the waste sample level (height); the change in level was then used to determine the magnitude of gas bubble retention (gas fraction). The second camera was typically located in the middle of the solids layer and focused on a 1–2-cm vertical segment of sample. These images provide detailed information on bubble shapes and the mechanisms of gas bubble retention. A Sekai ISC-800A color zoom video camera and an Imaging & Sensing Technology 200 M, model ETV-1258 radiation-hardened black-and-white zoom camera were used. The camera signals were displayed on two video monitors and recorded by two S-VHS format time-lapse videocassette recorders. These were typically operated in 24-hour mode, and the signals were recorded on 120-minute S-VHS tape. A date and time stamp was recorded simultaneously, and before each experiment the time was synchronized to within one second of the pressure data acquisition system time. Post-experimentally, still frame images were captured from the video tape records and printed with a Sony UP-5600 MD Color Video Printer.

Some of these images are presented in the gas retention results sections (4.2, 4.3, and 4.4). The color photographs of gas bubbles in the various tank samples presented throughout this section generally do not reflect the colors of the actual waste. The reproduced colors are affected by the lighting conditions in the hot cell and the digital enhancement process used to generate the photographic prints from the videotape. Waste color is not used as a measure or indicator in these studies; the images are color because of the video equipment used.

4.1.4 Void Fraction Definitions and Gas Release Detection

The change in total sample volume from atmospheric pressure to some reduced pressure is defined here as the growth volume of retained gas within the nonconvective solids layer; this accounts for both particle-displacing and interstitial liquid-displacing bubbles within the solids fraction. The solids layer growth void fraction is the growth volume divided by the volume of the bubble-laden nonconvective layer at the same instant. The maximum growth void fraction reflects the peak sample growth. Growth void fractions are not the absolute void fractions

within the sample, because any gas initially present within the solids layer is neglected. The uncertainty of growth void fraction estimates is dominated by the uncertainty of the waste level measurement, particularly for samples with an uneven surface free of supernatant liquid. Waste levels are recorded to the nearest 0.05 cm, but in some cases the uncertainty in the observed level may be as great as 0.2 cm. For a typical sample (12.5 ± 0.05 cm initial; 20 cm ± 0.2 cm final), the calculated error in growth void fraction is ~0.01.

A method based on the ideal gas law has been applied to estimate the volume of retained gas initially present in the sample (Gauglitz et. al. 1996; Rassat et al. 1997). In this technique the growth volumes early in an evacuation experiment (e.g., P > 400 mm Hg) are plotted against the inverse pressure, and the slope of the line (m = PV = nRT, ideal gas) is used to calculate an initial volume of gas retained ($V_i = m/P_i$). The initial gas volume may be overestimated using this approach because initially dissolved gases may also contribute to the volume expansion that results from sample evacuation. Therefore, this estimated initial gas volume is an upper bound. Any reported absolute void fractions have been computed as the sum of the estimated initial and measured growth volumes divided by the observed bubble-laden solids volume.

The ideal gas law has also been applied to detect gas release from experimental samples (Gauglitz et. al. 1996; Rassat et al. 1997). The ideal gas law relationship

$$V_2 = V_1 \frac{P_1}{P_2} \tag{4.2}$$

is employed. Strictly speaking, the volumes V_1 and V_2 are absolute gas volumes. Here, however, V_1 is defined as the growth volume at system pressure P_1, and V_2 is the expected growth volume when the pressure is changed to P_2. When gas is completely retained by the sample, the actual measured growth volume resulting from the pressure change should be greater than the estimated value, V_2, because the absolute volume of retained gas is greater than the growth volume. Therefore, if V_2 exceeds the measured growth volume, gas release is indicated. In subsequent steps, V_1 is reset to the current measured growth volume, and a new V_2 is estimated. Since the absolute volume of retained gas is not used in this calculation, the method cannot be used to calculate gas release volumes. It is only applied as a gas release indicator.

4.2 Tank A-101

A discussion of the gas bubble retention mechanisms and results for sample S97M000176 from Tank A-101, Core 154, segment 5 is presented in this section. This particular A-101 sample was used in previous RGS testing (Shekarriz et al. 1997). The A-101 sample was the only temperature-controlled sample (~53°C) in the four gas retention experiments described here. Unfortunately, the temperature control system experienced difficulties during the sample settling period. The in-cell water recirculation pump used to pump water through the jacketed vessel failed three times during the four-week sample settling period; twice the original pump was

disassembled and fixed in-cell using manipulators, and finally it was replaced. During the 24-hour evacuation experiment and for several days before that, the elevated temperature was maintained. The supernatant liquid that surfaced during the settling period was removed before the A-101 sample evacuation to eliminate neutral buoyancy as a possible mechanism for gas release in these tests. The density of the supernatant liquid was measured and is reported in Section 4.5.

4.2.1 Retention Mechanisms

The upper-left photograph in Figure 4.2 shows the retained bubbles within the A-101 sample prior to sample evacuation. This close-up photograph and the others in Figure 4.2 suggest the waste in this A-101 sample is a relatively fine-grained, moist salt. The center of the field of view in the photographs is about 6 cm above the bottom of the retention vessel, corresponding to roughly half the initial height of the solids layer. For reference, the retention vessels are grooved every 0.5 cm along their height. In spite of the RGS history of this sample and the fact that ii was not irradiated with a cesium gamma source before evacuation, a surprising amount of gas was generated and observed in the retention vessel prior to evacuation. As the pre-evacuation image in Figure 4.2 shows, clusters of round gas bubbles, approximately 100 microns in diameter, were distributed throughout the waste column. A few bubbles about 0.5 mm in diameter are also seen in the photograph. Assuming uniform distribution of the smaller bubbles through the 2.54-cm (1-in.)-diameter vessel, about 10% gas volume fraction was estimated from the visual data. The generation of bubbles in the sample was suspected to be the result of the thermal history of the material. After sample receipt in the 325A HLRF (and presumably since retrieval from the tank) the sample was stored at ambient hot cell conditions (26–30°C); for shear strength testing, the sample was heated to 55°C for about two days, and then cooled and held at ambient temperature for about a week before it was mixed and added to the retention vessel. The bubbles were detected several days after the retention vessel was brought to temperature (~53°C). Because of the number of bubbles and the uniformity of the distribution, it is believed that these bubbles were not entrained while loading the vessel. Rather, reduced gas solubility at elevated temperatures seems the most plausible explanation. The sample did not appear to grow (generate and retain additional gas) when held at elevated temperature during the four-week settling period. Level growth and pressure data from early in the evacuation experiment were used to estimate a 6% initial gas fraction, slightly lower than estimated by visual means. The estimated initial gas content is defined as 0% growth.

The other three pictures in Figure 4.2 show the retained bubbles within the A-101 sample at various stages of the gas retention experiment. The photograph at the upper right was taken approximately six hours after the start of evacuation and represents 10% gas volume growth in the solids layer. At this stage, the bubbles are still essentially round with only minor distortion and elongation. The lower-left photograph, taken approximately 12 hours into the experiment, represents 21% gas volume growth. The typical size of the bubbles increased to approximately

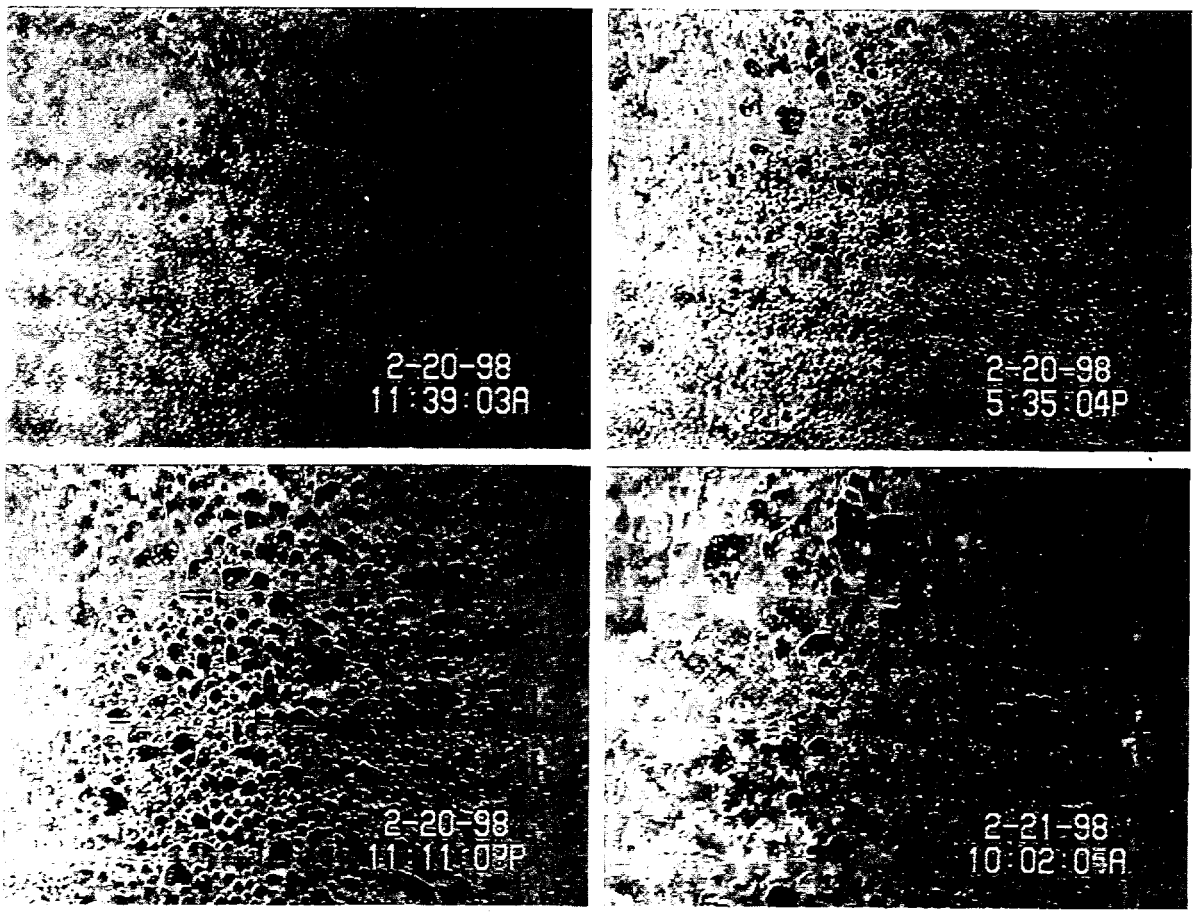

Figure 4.2. Gas Bubbles in A-101 as a Function of Gas Fraction. (UL) pre-evacuation (0% growth); (UR) 10% gas volume growth; (LL) 21% gas volume growth; and (LR) 36% gas volume growth

0.5 mm in diameter, with some nearly 2 mm. Generally, the bubbles also appear to be more distorted and elongated. In bentonite clay simulants (Gauglitz et al. 1996), the round and distorted-round bubbles indicate a waste of moderate strength (~50 Pa). In weaker materials, only round bubbles are expected, and in strong materials, highly distorted, particle-displacing, dendritic bubbles are the norm. The lower right photograph, taken almost 23 hours after the start of evacuation, represents the maximum gas retention condition in which the gas volume growth was 36%. Some larger bubbles are observed at the highest gas fraction; in particular, there is a 4-mm-diameter distorted bubble near the top center of the photograph. Overall, however, fewer bubbles are visible in the lower right frame in spite of the higher measured gas fraction. This represents a condition in which a majority of the gas bubbles are out of view because of a thin waste layer at the vessel interface.

4.2.2 Quantitative Results

The growth gas fraction data for the A-101 sample are plotted as a function of pressure in Figure 4.3. In this day-long experiment (P_{init} = 760 mm Hg, t_{set} = 180 minutes), a maximum gas volume growth of 36% was measured at a pressure of 89 mm Hg (0.084 kPa^{-1}) after approximately 23 hours elapsed time. For comparison, the RGS in-tank gas fraction of this core segment was approximately 14% (Shekarriz et al. 1997). However, RGS measurements are not intended to measure the maximum fraction of gas that could be attained, as is the case in the gas retention experiments. Figure 4.3 also includes projected gas fraction data assuming ideal gas law behavior in the retained gas. The estimated retained volume at some pressure, P_1, is used to predict the volume at the next measured pressure, P_2 (see discussion in Section 4.1.4). When the measured growth volume is less than predicted, gas release is implied.

As shown in Figure 4.3, the A-101 sample volume (and gas fraction) increases essentially linearly with the inverse pressure up to a growth gas fraction of about 0.21. At this point, the slope of the growth curve decreases very slightly and then increases up to a growth fraction of approximately 0.25. This time period correlates to a gas release that was observed visually with the close-up video camera and confirmed by the fact that the measured growth volume is less than predicted. After this event, the sample volume continued to increase linearly with the inverse pressure up to the point of maximum growth, after which gas was released again and the

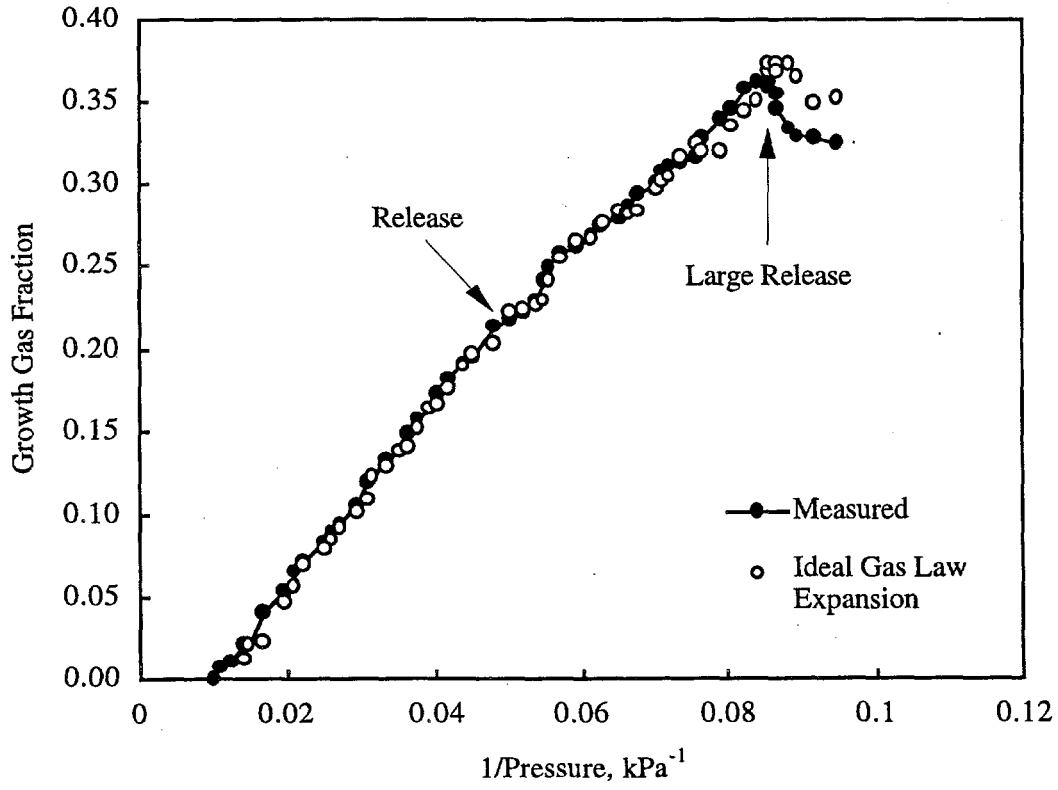

Figure 4.3. Gas Retention and Release for a Tank A-101 Sample

retained gas volume decreased. Approximately 15% of the retained gas volume was released, corresponding to a retained gas fraction drop of less than 0.04, as the vessel pressure was reduced from 89 mm Hg (0.084 kPa^{-1}) to 79 mm Hg (0.095 kPa^{-1}). The growth profile in Figure 4.3 is similar to those observed in previous simulated waste gas retention studies using moderately weak (~67 Pa) bentonite clay sludges as well as in previous maximum gas retention studies conducted on saltcake samples from SST S-102 (Gauglitz et al. 1996). These previous studies showed that both the maximum retention and the retention and release characteristics were dictated by the material strength. Due to differences in physical, chemical, and rheological properties between the clay simulants and the actual tank waste, no direct correlations can be made; however, the simulant and actual waste results indicate consistent behavior at comparable estimated strength. See Section 5 for additional discussion.

4.3 Tank S-106

A discussion of the gas bubble retention results for sample S97T000383 from Tank S-106, Core 183, segment 8 is presented in this section. As in the A-101 sample, the small amount of supernatant liquid that surfaced during the settling period was removed prior to sample evacuation. The density of this liquid was measured and is reported in Section 4.5.

4.3.1 Retention Mechanisms

Figure 4.4 shows the retained bubbles within the S-106 sample at different levels of retention. The center of the field of view in the photograph is about 8.5 cm above the bottom of the retention vessel, corresponding to roughly 70% of the initial height of the solids layer. The upper left section of the figure is an image obtained before sample evacuation (0% growth). This photograph and the others in Figure 4.4 suggest that the tested S-106 sample is a relatively fine-grained moist salt. Visually, the material appears loosely packed, almost fluffy, but waste density measurements do not indicate significant differences from the A-101 salt sample tested (see Section 4.5). Even though the S-106 sample was not irradiated with a gamma source prior to evacuation, level changes early in the evacuation indicated a high apparent initial gas fraction (~8%). This is higher than that observed in the A-101 sample, although visually the bubbles were not as obvious in the S-106 sample. A thermal cycling mechanism was postulated to explain the high initial gas content in the A-101 sample; however, the S-106 sample was held at the ambient hot cell temperature (26–30°C) throughout the experiment. Gas bubble entrainment in the vessel loading process is a possible explanation for the high initial gas volume.

The upper right photograph in Figure 4.4 was taken approximately 4.5 hours after the start of evacuation and represents 15% gas volume growth in the solids layer. At this stage, the bubbles are still essentially round, with only minor distortion and elongation in the larger bubbles (~1-mm diameter). The lower left photograph, taken approximately 11 hours into the experiment, represents 31% gas volume growth. The typical size of the bubbles increased to approximately 0.5 mm, with some almost as large as 2 mm. The lower right photograph, taken

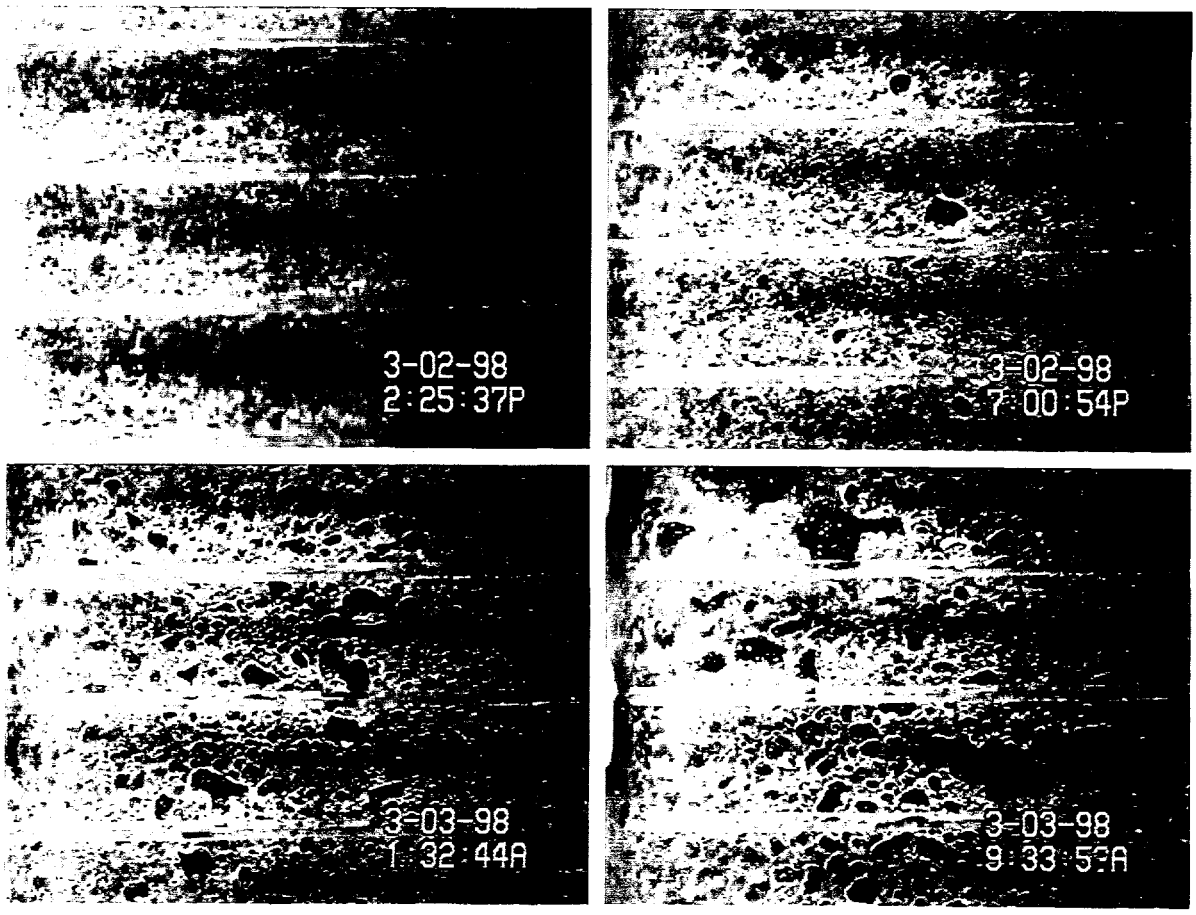

Figure 4.4. Gas Bubbles in S-106 as a Function of Gas Fraction; (UL), pre-evacuation (0% growth; (UR), 15% gas volume growth; (LL), 31% gas volume growth; and (LR), 47% gas volume growth

about 19 hours after the start of evacuation, represents the maximum gas retention condition, in which the gas volume growth was 47%. The typical bubble size increased to about 1 mm in diameter, with bubbles as large as 5 mm observed. The larger bubbles appear significantly distorted, indicative of a moderate strength material (Gauglitz et al. 1996).

4.3.2 Quantitative Results

The retention data for the S-106 sample are plotted as a function of pressure in Figure 4.5. In this experiment (P_{init} = 760 mm Hg, t_{set} = 120 minutes), a maximum gas volume growth of 47% was measured at a pressure of 70 mm Hg (0.107 kPa^{-1}) after approximately 19 hours elapsed time. For comparison, the RGS in-tank gas fraction of a sample from segment 6 of Core 183 (taken approximately 95 cm above the sample used for gas retention testing) was approximately

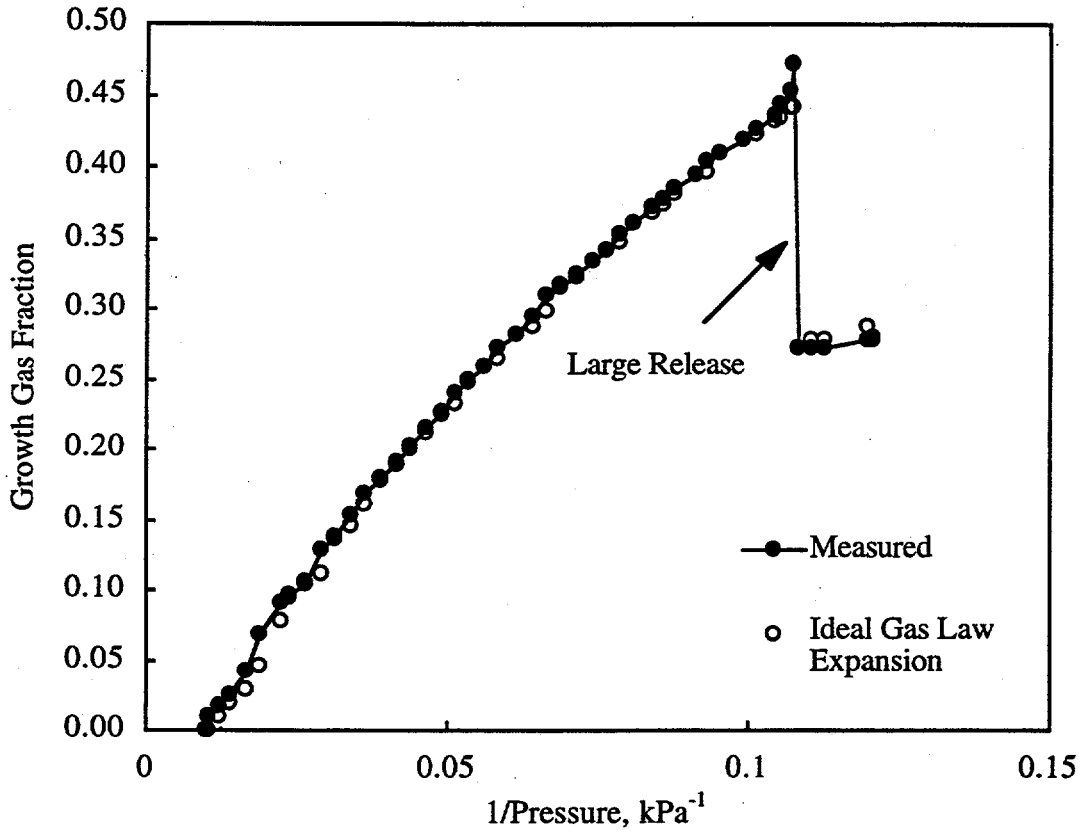

Figure 4.5. Gas Retention and Release for a Tank S-106 Sample

7% (Mahoney et al. 1997). However, as previously indicated, RGS measurements are not indicative of the maximum gas retention that could be attained. To detect gas release from the sample, the ideal gas law volume growth prediction technique was applied. The equivalent ideal gas law estimated growth gas fractions are shown with the experimental data in Figure 4.5, and when these exceed the measured growth datum at a given pressure, gas release is implied. As is evident in the figure, the sample volume (and gas fraction) increased essentially linearly with the inverse pressure up to the point of maximum growth. This behavior is characteristic of the ideal gas law.

Although the visual appearance and gas retention behavior of the S-106 sample is similar to that observed in the A-101 experiment and earlier experiments with S-102 saltcake composite (Gauglitz et al. 1996), the gas release behavior in the S-106 material was somewhat different. As is evident in Figure 4.5, upon reaching its maximum gas retention, the S-106 sample level collapsed almost instantaneously from about 22 cm to 16 cm, resulting in a retained gas fraction decrease from ~0.5 to ~0.3. This corresponds to a release of more than 50% of the retained gas volume from the sample. In the replicate S-102 saltcake tests, the samples cyclically released only small quantities of gas (~10% of retained volume [Gauglitz et al. 1996]) after reaching

maximum retention. These differences in release behavior may reflect differences in waste sample strength, as was previously observed in bentonite clay simulant studies (Gauglitz *et al. 1996*). Weak clays (~30 Pa and weaker) showed more rapid and larger gas releases like the S-106 sample, while somewhat stronger clays (~70 Pa) had smaller releases like those in A-101 and S-102 saltcake samples. Section 5 of this report describes this phenomenon in greater detail.

4.4 Tank U-103

A discussion of the gas bubble retention results for samples S97M000224 and S97M000225 from Tank U-103, Core 182 are presented in this section. As in the other SST samples, the small amount of supernatant liquid that surfaced during the settling period was removed from both U-103 composite samples prior to sample evacuation. The densities of the supernatant liquids were measured and are reported in Section 4.5.

4.4.1 Retention Mechanisms

Figure 4.6 shows the retained bubbles within the U-103 upper-tank composite sample (segments 1 and 2, Core 182) at various stages of the gas retention experiment. The center of the field of view in the photographs is about 8.5 cm above the bottom of the retention vessel, corresponding to roughly 60% of the sample height. Close-up images of the sample show that the waste is composed of smaller particles than samples from A-101 and S-106. Mahoney et al. (1997) described segment 1 as sludge slurry and segment 2 as salt slurry, which is consistent with our observation of a very fine-particulate composite material. The upper left photograph shows the pre-evacuation condition with an initial gas content of 2% (defined as 0% growth) estimated by level changes early in the evacuation. This initial gas fraction was more in line with that expected for a sample that was not irradiated with a cesium gamma source, in contrast to the surprisingly high initial gas volumes found in the A-101 and S-106 samples. As a result of the lower initial gas fraction, the gas bubbles are not as evident as they were in the pre-evacuation A-101 and S-106 photographs. The upper right photograph was taken approximately 3.5 hours after the start of evacuation and represents 10% gas volume growth in the solids layer. At this stage, the median bubble size has increased to about 0.5 mm in diameter, and most of the bubbles are still essentially round, with only minor distortion and elongation in the larger bubbles. The lower left photograph, taken about 6.5 hours into the experiment, represents approximately 20% gas volume growth. Here, the typical size of the bubbles increased to approximately 1 mm, and more of the bubbles appear to be distorted and elongated. The lower right photograph was taken about 27 hours after the start of evacuation and just moments after a moderate gas release. The gas release followed a relatively rapid growth spurt in which the maximum growth gas fraction of 28% was reached. The waste in the lower right photograph is at a growth gas fraction of approximately 26%, just shy of the maximum. In spite of the larger measured gas fraction in the image depicted on the lower right of the figure, the waste appears to have less retained gas than in the lower left photograph. This is due to waste smearing the vessel walls during the gas release and emphasizes the care that must be taken in using visual data to estimate gas content.

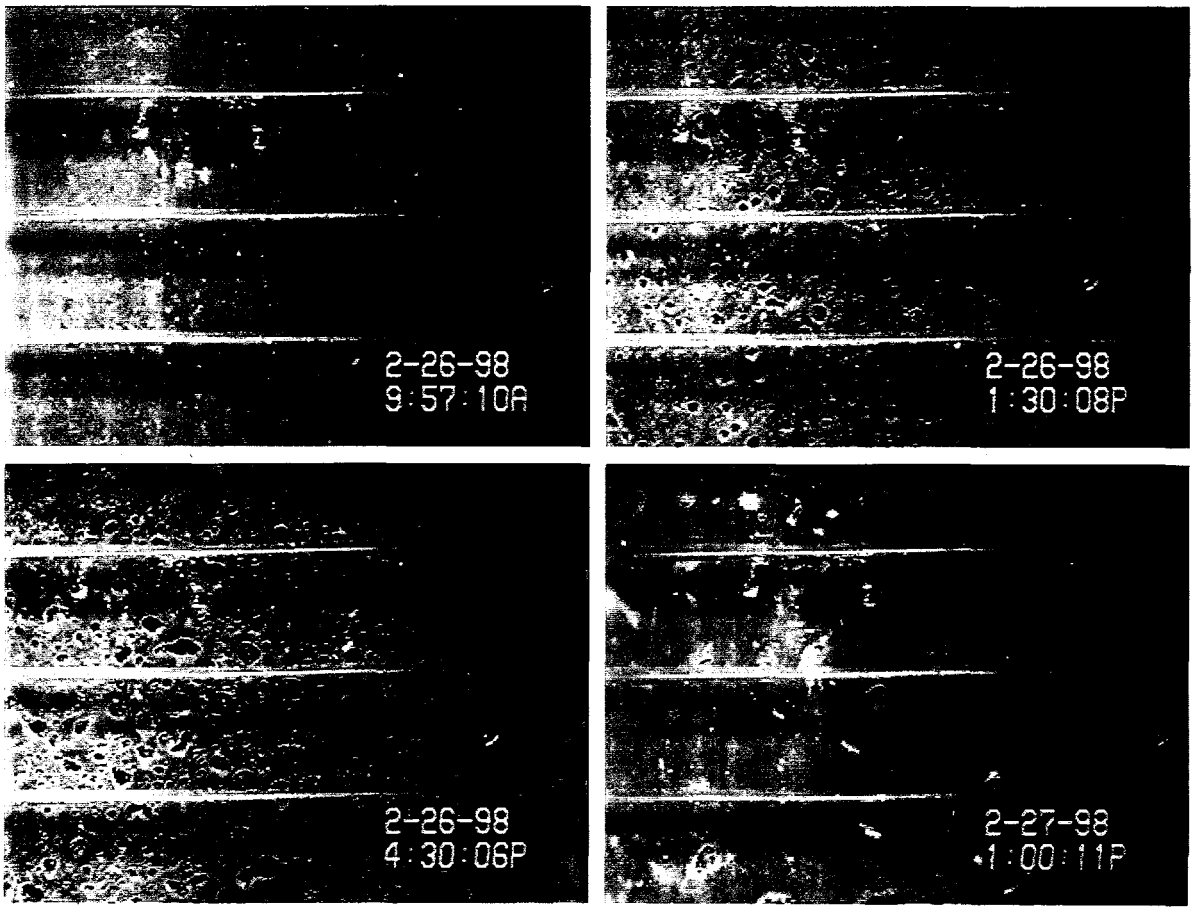

Figure 4.6. Gas Bubbles in U-103 Upper Tank Composite Sample as a Function of Gas Fraction; (UL), pre-evacuation (0% growth); (UR), 10% gas volume growth; (LL), 20% gas volume growth; and (LR), 26% gas volume growth

Figure 4.7 shows the retained bubbles within the U-103 middle-tank composite sample (segments 5 and 6) at various stages of the gas retention experiment. The center of the field of view in the photographs is about 8.5 cm above the bottom of the retention vessel, corresponding to roughly 60% of the sample height. In these close-up images, the waste looks very similar to the U-103 upper-tank composite sample in Figure 4.6, and again is characterized as a very fine-particulate material. The upper left photograph shows the pre-evacuation condition, with an initial gas volume of 2% estimated by level changes early in the evacuation (0% growth). As was the case with the pre-evacuation image in Figure 4.6, very few bubbles are visible. The upper right photograph was taken almost four hours after the start of evacuation and represents 11% gas volume growth in the solids layer. The typical bubble size is smaller than depicted in the upper right frame of Figure 4.6 (at a volume content of ~10%); however, there are more bubbles in the U-103 middle-tank composite sample. The lower left photograph, taken about nine hours into the experiment, represents approximately 25% gas volume growth. The typical bubble increased to approximately 1 mm in diameter, and more appear to have a distorted shape. The

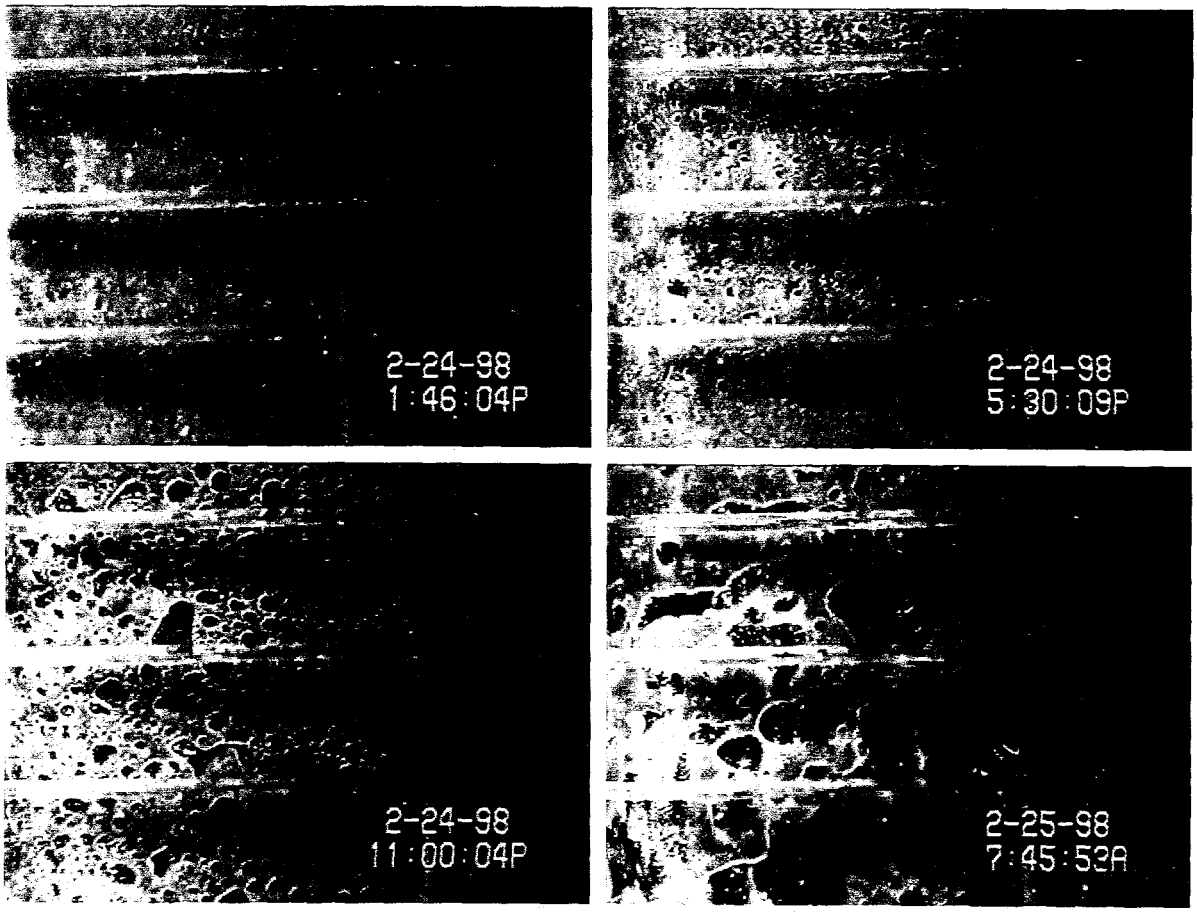

Figure 4.7. Gas Bubbles in U-103 Middle Tank Composite Sample as a Function of Gas Fraction; (UL), pre-evacuation (0% growth); (UR), 11% gas volume growth; (LL), 25% gas volume growth; and (LR), 42% gas volume growth

lower right photograph was taken about 18 hours after the start of evacuation and represents the maximum gas retention condition, where the gas volume growth was 42%. It is clear that the size of the bubbles has increased dramatically to almost 5 mm, and most of them are non-spherical. The gas retention behavior depicted in these photographs is similar to that observed in previous simulated waste gas retention studies using moderately weak (~67 Pa) bentonite clay sludges (Gauglitz et al. 1996) and suggests the U-103 waste sample is of moderate strength (see Section 5).

Figure 4.8 compares the two U-103 waste samples at the same gas fraction (20% growth). The upper photograph is the U-103 upper-tank composite sample (segments 1 and 2), and the lower shows the U-103 middle-tank composite sample (segments 5 and 6). The figure shows

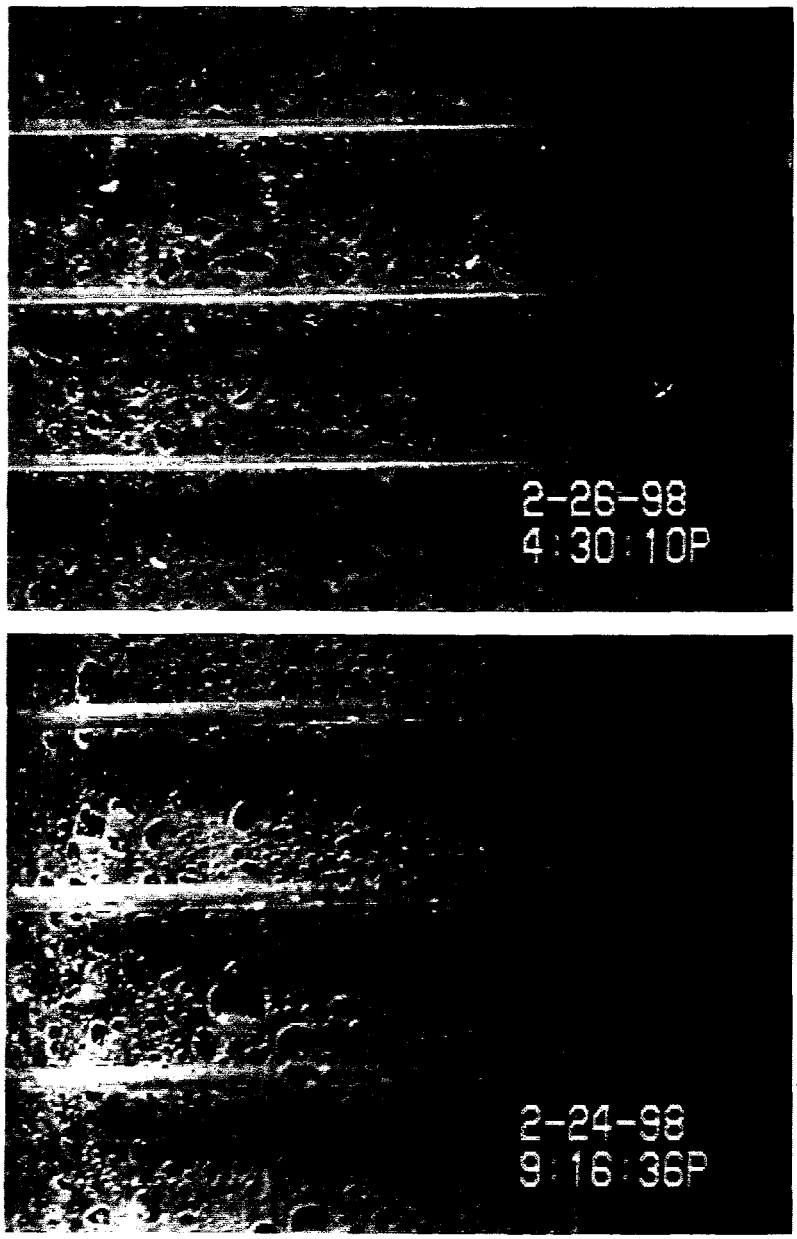

Figure 4.8. Gas Bubbles in Tank U-103 Upper (upper photograph) and Middle-Tank Segment Composites at 20% Gas Volume Growth

great similarity in the two samples at the same gas fraction and indicates that the samples have comparable strengths. In fact, the gas retention and release behaviors of the two samples were very similar except for their maximum growth gas fraction (0.28 in upper and 0.42 in lower). The difference in maximum retention is not clearly understood; it is discussed further in Section 4.4.2.

4.4.2 Quantitative Results

The gas retention profiles for the two U-103 composite samples are plotted in Figure 4.9. In the U-103 upper-tank composite experiment (P_{init} = 760 mm Hg, t_{set} = 40 minutes), a maximum gas volume growth of 28% was measured at a pressure of 49 mm Hg (0.154 kPa^{-1}); in the U-103 middle-tank composite experiment (P_{init} = 760 mm Hg, t_{set} = 40 minutes), a maximum gas volume growth of 42% was observed at a pressure of 27 mm Hg (0.278 kPa^{-1}). The slopes of the growth curves for the two samples are similar, but they do not overlap. The slightly increased slope in the upper-tank composite sample (filled circles) may reflect higher concentrations of dissolved gas (e.g., ammonia) that evolve during depressurization.

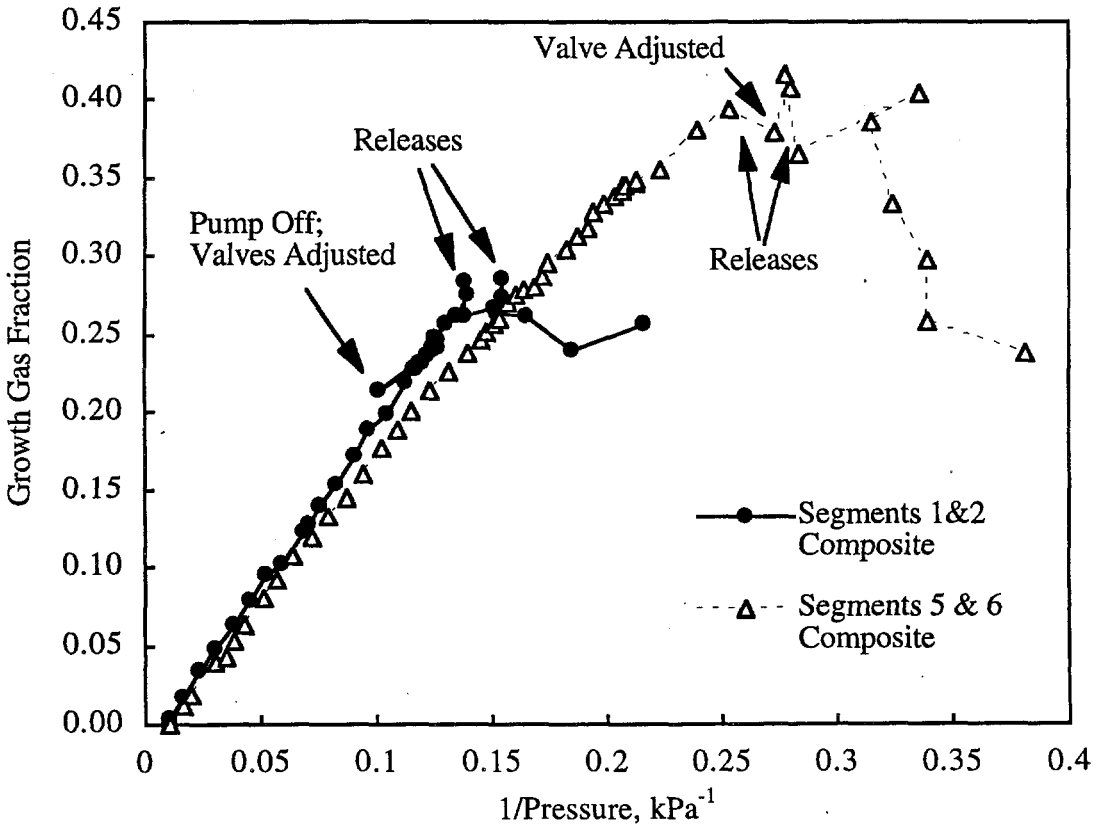

Figure 4.9. Comparison of Gas Retention and Release in U-103 Upper and Middle-Tank Composite Samples

Unfortunately, during the unmanned evening hours of both U-103 composite tests, the vacuum pump was unable to maintain the set-point pressures because of unexpectedly high leak rates through the system bleed valve. Pre-experiment testing indicated that the vacuum capacity of the system was more than sufficient to maintain set-point pressures with the normal bleed valve adjustment (~1/2 turn open or less). Apparently, degradation of the valve seal led to increased leakage at a fixed valve opening. During the U-103 upper-tank composite test from about 5 p.m. on February 26 until about 10 a.m. on February 27, 1998, the system pressure remained constant at about 60 mm Hg, even though the set-point pressure had continued to decrease linearly to a pressure of about 20 mm Hg. During the U-103 middle-tank composite test, from about 3 a.m. until about 7:40 a.m. on February 25, 1998, the system pressure remained constant at about 36 mm Hg, even though the set-point pressure had continued to decrease linearly to a pressure of about 27 mm Hg. When these situations were discovered, the valve system was adjusted, and the pressure control programs were restarted. This resulted in less than ideal pressure swings. The outlier point (1/P = 0.102, gas fraction = 0.22) on the U-103 upper-tank composite linear growth curve occurred when the pump was temporarily isolated from the vessel and the bleed valve system adjusted. The system pressure jumped from about 60 mm Hg to about 73 mm Hg. It took about nine minutes to reestablish the set-point pressure, and shortly after this, the waste experienced the two sudden growth spurts/gas releases that are evident in Figure 4.9. The maximum growth gas fraction of 28% was achieved at the peak of the second growth spurt. In the U-103 middle-tank composite sample, after the bleed valve was adjusted, the system pressure immediately decreased and the waste experienced a large growth spurt. The maximum growth gas fraction of 42% was achieved at the peak of this growth spurt.

Previous studies (Rassat et al. 1997) investigated the effect of the length of the experiment on the maximum gas retention and found that there was little variance for experiments lasting from a few hours to a few days, suggesting that the overnight delay experienced during the two U-103 experiments should not have corrupted the results. However, in the case of the U-103 upper-tank composite sample, the large pressure fluctuation that occurred when the valve system was adjusted may have affected the results and could explain the abnormally low maximum growth gas fraction. In spite of these pressure fluctuations, the growth profiles in the figure are similar to those observed in other samples. The profiles are characteristic of moderate strength bentonite clay (~50 Pa), although the somewhat larger release in the middle-tank composite sample (open triangles) following maximum retention is characteristic of a slightly weaker material. About 50% of the retained gas volume in the middle-tank composite was lost as the growth gas fraction decreased from 0.38 at 24 mm Hg (0.31 kPa^{-1}) to 0.24 at 20 mm Hg (0.38 kPa^{-1}). This release activity may have been precipitated by the vacuum system adjustment discussed above. The gas release in the U-103 upper-tank composite sample was considerably smaller, with ~20% retained gas volume decrease corresponding to a retained gas fraction drop of ~0.04.

As discussed in Section 2, the main reason for testing two different composite samples from Tank U-103 was that RGS measurements indicated an inverted gas inventory, with upper-tank samples showing higher gas retention than lower-tank samples. Mahoney et al. (1997) reports a gas volume fraction of 44% in a sample from Core 176, riser 7, 360 cm above the tank center,

while gas volume fractions of about 10% were measured in samples from the same riser at elevations below 220 cm. These data are in good agreement with x-ray data obtained on the same samples. X-ray data for another RGS sample from Core 182, riser 13 at an elevation of about 320 cm indicated a visible gas fraction of 47% (RGS measurements were not obtained for this sample because the sampler valve froze closed after the sample was taken). This RGS sample was immediately above the U-103 middle-tank gas retention sample (Core 182, segments 5 and 6) that gave a maximum total gas fraction of 43%. (The maximum total gas fractions measured in the current experiments include the estimated initial gas volumes. See Section 4.5 for additional discussion of the definitions of growth and total gas fractions.) Figure 4.10 summarizes the RGS, x-ray, and gas retention results for Tank U-103.

Maximum gas retention measurements for the two U-103 composite samples do not provide evidence to rationalize the inverted gas inventory observed in the RGS samples. The U-103 upper-tank gas retention sample (Core 182, segments 1 and 2) gave a maximum gas fraction of

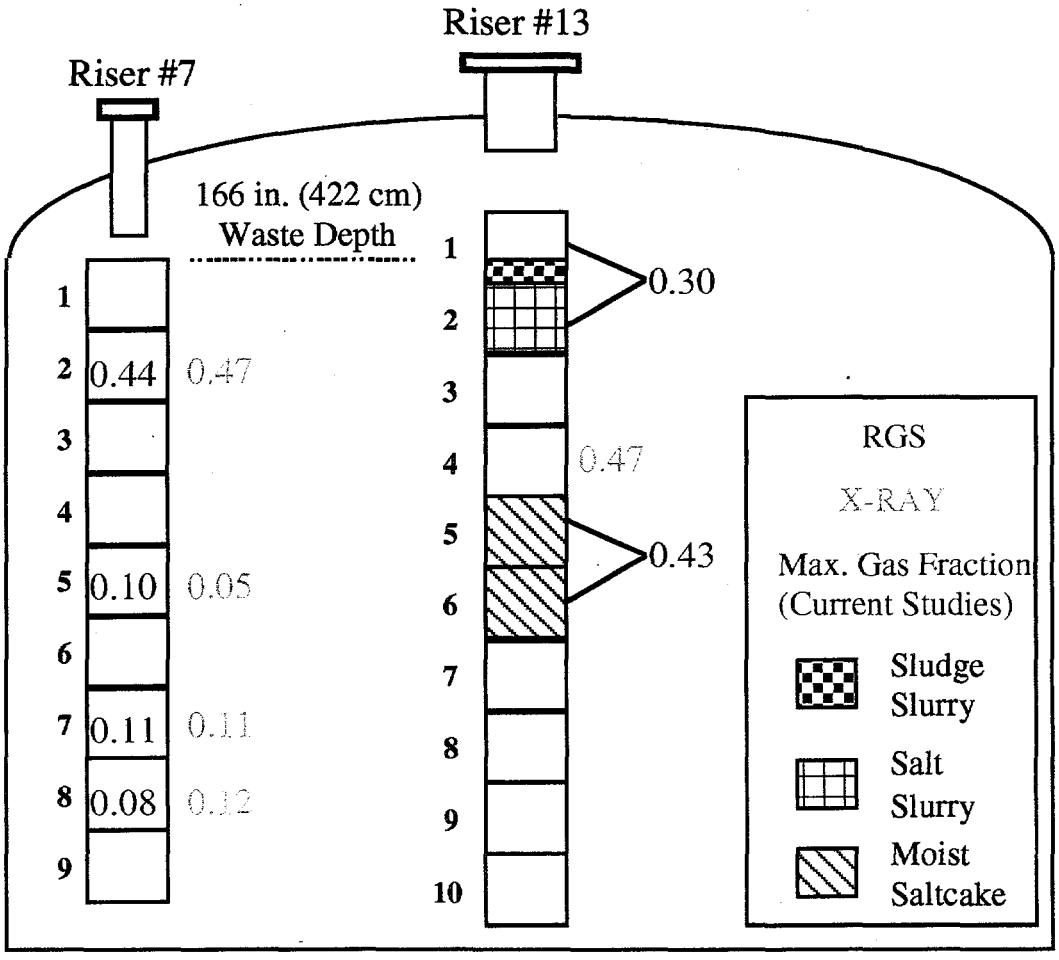

Figure 4.10. Summary of U-103 Gas Fraction Results from Previous RGS and X-Ray Analyses and Current Gas Retention Testing

about 30%, less than the 43% observed in the middle-tank sample. However, the gas retention samples came from a different lateral location in the tank than the RGS samples, and it appears that retained gas fractions in U-103 vary appreciably with both lateral and vertical position. RGS measurements are not an indication of maximum gas retention, but the RGS results show gas inventories in some tank locations comparable to the measured maximum retention value, which suggests that a near-maximum retention condition may exist in some portions of the tank.

4.5 Summary of Gas Retention Results

Gas retention results for the four experiments conducted on A-101, S-106, and U-103 waste samples are summarized in Table 4.1, including estimated initial gas contents (pre-evacuation), measured maximum gas growth fractions, and estimated total maximum gas fractions. The last quantity is determined by considering both measured maximum sample growth and estimated initial gas content. Measured sample growth during the initial stages of the evacuation experiments and application of the ideal gas law resulted in initial gas content estimates of 2 to 8%. Samples from A-101 and S-106 exhibited surprisingly large initial gas volume fractions (6 and 8%, respectively); the two U-103 samples each contained approximately 2% initial gas. Measured maximum growth gas fractions ranged from 28 to 47%, and the estimated absolute gas fractions were 1 to 4% greater in each sample. Note, however, that the relatively low maximum retention in the U-103 upper-tank composite (0.30 gas fraction) may be the result of the pressure control correction made during the experiment (Section 4.4.2). Neglecting this result as anomalous, the range of maximum gas fractions is narrowed considerably (0.40–0.51).

Waste strength is considered to be a primary determinant of gas retention capacity in SST wastes containing particle-displacing bubbles. The gas retention profiles for all four samples resembled those from simulated waste gas retention studies using moderate strength (~30–70 Pa) bentonite clays (Gauglitz et al. 1996), and this indicates relatively consistent strength in the SST

Table 4.1. Summary of Gas Retention Data for A-101, S-106, and U-103 Samples

Tank	LabCore #	Initial Gas Content, % (ideal gas law)	Measured Max. Gas Growth Volume, %	Estimated Total Max. Gas Fraction, %	Supernatant Liquid Density, g/mL	Initial Settled Solids Density, g/mL	Minimum Waste Density, g/mL
A-101	S97M000176	6	36	40	1.61 ± 0.06	1.71	1.09
S-106	S97T000383	8	47	51	1.57 ± 0.04	1.74	0.92
U-103 (upper)	S97M000224	2	28	30	1.42 ± 0.13	1.70	1.21
U-103 (middle)	S97M000225	2	42	43	1.58 ± 0.07	1.78	1.04

test materials. Because there is some variation in maximum retention in these actual waste samples of apparently similar strength, the significance of other waste properties in maximum retention in SST wastes should be examined. Properties of merit include chemical composition, particle size distribution, colloidal properties, surface tension, and density. Of these, only density data are readily available. Supernatant liquid and initial settled solids density data were obtained for each waste sample, and these are reported in Table 4.1. As indicated in Section 4.1.1, the reported uncertainties in the liquid density were propagated from the estimated variability of the mass and volume measurements. Larger uncertainties correspond to reduced sample size; in the case of the U-103 upper-tank composite sample, only 1.1 mL of liquid was available and a large error in the density is estimated (±0.13 g/mL). Uncertainties in the pre-evacuation settled solids densities (not corrected for initial gas) were determined by propagating estimated uncertainties in sample mass, volume, and liquid density. In all cases, the uncertainty in the initial settled solids density was estimated to be about 0.02 g/mL.

In the limited U-103 experiments, the upper-tank segment composite had both a lower settled solids density (1.70 g/mL) and lower maximum growth gas fraction (0.28) than the middle-tank segment composite (1.78 g/mL settled solids density and 0.42 maximum growth gas fraction). As noted above, however, the differences in maximum retention of U-103 composite samples may be an anomaly resulting from an experimental upset rather than due to physical or chemical differences in the samples. If all four SST waste samples are considered, there is no obvious correlation of either the supernatant liquid density or the initial settled-solids density values and maximum retained gas. In Table 4.1, estimated values of the bubble-laden sample density at the point of maximum retention (i.e., the minimum density) are reported. Not surprisingly, these minimum density values are a good indicator of the maximum retained gas fraction. The S-106 sample with the largest maximum gas fraction (0.51) had the lowest density (0.92 g/mL), while the U-103 upper-tank composite sample had the smallest maximum gas fraction (0.30) and the highest density (1.21 g/mL). There does not appear to be a consistent limiting value of the minimum sample density (e.g., 1.0 g/mL) beyond which the sample is not able to retain more gas. The correlation of gas retention and release characteristics with waste properties is addressed further in Section 5.

Waste sample density information can be used to evaluate the in-tank gas retention condition reported for A-101 (Shekarriz et al. 1997), which indicates an inverted waste configuration (i.e., the nonconvective solids layer is floating on the convective liquid layer). Using the A-101 gas retention sample density measurements (supernatant liquid: 1.61 g/mL; bulk waste at 0.06 gas fraction: 1.71 g/mL), it was estimated that the waste sample nonconvective material would have become neutrally buoyant (floated) at a gas fraction of 0.12 or greater if enough supernatant liquid had been present. This is consistent with the RGS gas fraction result of 0.14 reported for the same core segment sample (Shekarriz et al. 1997). The higher measured maximum retention (0.40 gas fraction) in the current studies suggests that more gas could possibly be retained in the floating solids layer of A-101.

5.0 Summary of Single-Shell Tank and Simulated Waste Gas Retention Experiments to Date

Experiments on SST waste configurations indicate that the maximum gas fraction retained in a sample and the mechanism of gas release are highly dependent on the waste strength. On the other hand, DST waste experiments with relatively thick supernatant liquid layers indicate that maximum gas retention is governed primarily by neutral buoyancy considerations and perhaps secondarily by waste strength effects (Gauglitz et al. 1996; Rassat et al. 1997). Actual and simulated SST waste gas retention experimental results, including previous studies, are summarized in this section. These data reiterate the experimental evidence that ties gas retention and release in SST samples to waste strength.

Figure 5.1 summarizes the effects of waste strength on gas retention and release characteristics in simulated and actual SST wastes. The figure includes the current experimental results for Tanks A-101, S-106, and U-103 as presented in Section 4 and reproduces previous results for S-102 waste samples and bentonite clay simulated wastes (Gauglitz et al. 1996). There are two primary components to the summary data in the figure: 1) a series of gas retention profiles for both actual and simulated wastes and 2) a central plot depicting the effect of waste strength on measured maximum gas fractions and the mechanisms of gas release.

The gas retention and release profiles shown in Figure 5.1 are plotted in the normal way with gas fractions as ordinate values. The abscissa values differ for simulated and actual waste experiments. In the bentonite clay tests, the elapsed time is plotted from the start of the retention experiment; for actual waste experiments, the inverse pressure, which is typically applied linearly in time, is used. A series of bentonite clay retention and release profiles is shown along the bottom of the figure. The experimental details differ somewhat from the actual waste tests (Gauglitz et al. 1996). In the clays, gas was generated within the sample through the decomposition of homogeneously dispersed hydrogen peroxide to create oxygen gas bubbles. The length of the clay tests was on the order of four hours; in S-102 tests the duration of the evacuation (gas generation) was on the order of two hours; retention tests of approximately one day are the current norm for actual waste experiments (Section 4). The similarities of the actual and simulated waste experiments outweigh these minor differences.

The clay retention profiles at the bottom of Figure 5.1 demonstrate the effect of waste strength on both the maximum retention and the characteristics of gas release. In a weak, 6.4-Pa clay, maximum retention was near 0.2 gas fraction. Upon reaching the maximum, essentially all gas was released rather suddenly, followed by additional growth and release cycles of comparable magnitude. This release mechanism is characterized pictorially on the central plot as a group of four separate round bubbles that release simultaneously. This shows that the gas bubble content in the waste is insufficient to create a connected gas path to the waste surface, but at some critical gas fraction the strength of the material is sufficiently destabilized that a gas release consuming all individual bubbles ensues. In even weaker materials, retained gas fractions are lower, and

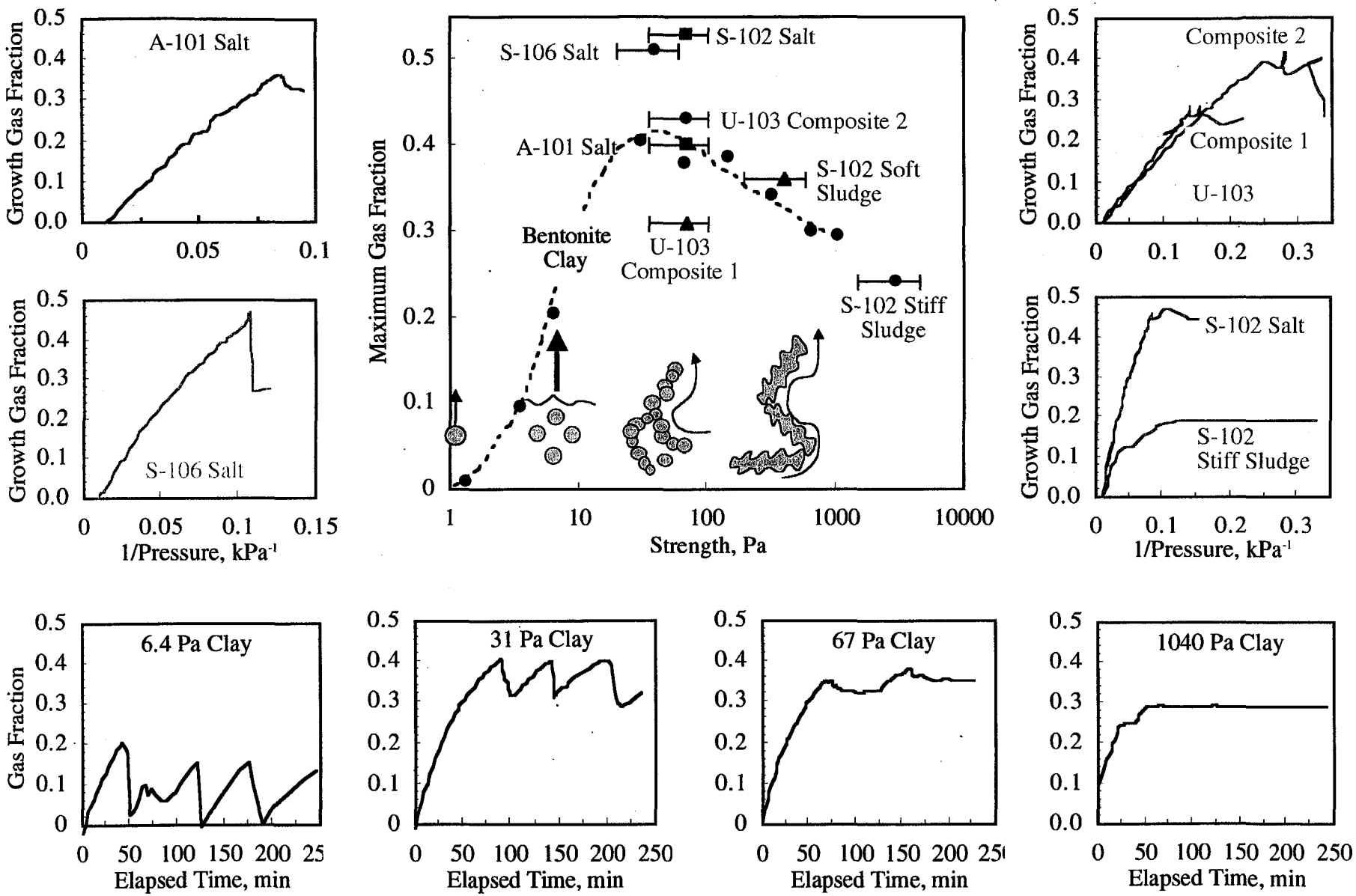

Figure 5.1. Effects of Waste Strength on Gas Retention and Release Characteristics in Simulated and Actual SST Wastes

individual round bubbles of sufficient dimension rise freely to the surface (Stewart et al. 1996). This release mechanism is also shown schematically on the lower left of the central plot.

As the strength of bentonite clays increases to moderate levels (of the order 50 Pa), the maximum gas retention increases to a gas fraction near 0.4. This is shown in the 31- and 67-Pa retention profiles in Figure 5.1. While the maximum retention is comparable in these samples, the profiles indicate a shift in the characteristics of gas release. The frequency and magnitude of gas releases is larger in the weaker material, suggesting a gas release mechanism comparable in many respects to the 6.4-Pa clay. The key distinction is that not all the sample is involved in the gas release from the 31-Pa material. After reaching a maximum gas content, a portion of the gas is released from the upper portion of the waste before the waste "heals" to retain subsequently generated gas. In the 67-Pa clay, however, the waste does not heal as readily. This is apparent in the minimum gas fraction plateaus that follow gas releases and reflects continual gas release from the sample until partial healing leads to renewed level growth. As shown in a drawing on the center plot of Figure 5.1, gas release in the 67-Pa clay is characterized by a connected path of distorted round bubbles that provide a nearly continuous path for gas release to the surface.

The maximum retained gas fraction in the strongest bentonite clay tested (1040 Pa) was lower (0.3) than that in the moderate-strength samples. The mechanism of gas release was also different (as indicated in Figure 5.1 in the gas retention profile for the sample and the depiction of bubble release in the center plot). Upon reaching the maximum retention, little change is detected in retained gas content, showing that gas is released continuously at the rate it is generated from that point forward. This phenomenon is accounted for by particle-displacing dendritic bubbles that form stable, connected paths to the waste surface at relatively lower gas fractions.

The SST actual waste results can be analyzed within the framework established for bentonite clay experiments. As noted in Section 1.2, materials in which retained gas bubbles displace particles may be considered continuum. As has been observed in SST actual waste gas retention experiments on both salt and sludge wastes, gas is retained primarily in particle-displacing bubbles, not interstitial liquid-displacing bubbles. Each of these wastes, like bentonite clay, demonstrates the properties of a continuum material. In a continuum material, the shape of a retained particle-displacing bubble is affected by the strength of the medium, the size of the bubble, and the surface tension force (Eq. 1.3). Bubble shape, in turn, is related to maximum gas retention and the mechanism of gas release, as discussed in conjunction with the bentonite clay retention profiles of Figure 5.1.

The gas retention experimental results obtained by Gauglitz et al. (1996) for two S-102 waste samples are reproduced on the right side of Figure 5.1. As discussed in that earlier report, four S-102 samples were tested, representing three physically distinct waste types: one was a stiff sludge; a second was a soft sludge; and the third was saltcake. The retention profiles for the strongest (stiff sludge) and weakest (a saltcake) S-102 wastes are shown in the figure. Similar to the bentonite clay results, the strength of the S-102 samples appears to affect both the magnitude of maximum gas retention and the character of the gas release. The relatively strong S-102 stiff sludge attained a maximum growth gas fraction of <0.2, whereas the weaker saltcake peaked at a

growth gas fraction near 0.5. Furthermore, the retention and release characteristics of the stiff sludge are comparable to the 1040-Pa bentonite clay shown in Figure 5.1. Both plateau at their respective maximum retention values, at which point any additional generated gas is continuously released. On the other hand, the S-102 saltcake results shown in Figure 5.1 more closely resemble the behavior of the moderate-strength (67-Pa) clay. Here, a series of small gas releases and regrowth is observed at near the maximum retention.

The gas retention profiles for A-101, S-106, and U-103 wastes, which are described in detail in Section 4, are duplicated in Figure 5.1. The profiles are similar in character to those for moderate-strength (31- and 67-Pa) bentonite clays. In S-106 saltcake, a rather sudden and relatively large gas release was detected after the maximum gas fraction, near 0.5, was reached. This is similar in nature to the release mechanism observed in the 31-Pa clay. The releases in A-101 saltcake and both U-103 composite samples were relatively smaller and characteristic of the 67-Pa clay.

The maximum gas retention values for each of the gas retention and release profiles depicted along the periphery in Figure 5.1 represent a single ordinate value on the center plot in the composite figure. For tank waste samples, the retention values in the center plot are the estimated total gas fractions at maximum retention, not the maximum growth fractions depicted in the side plots. The difference, accounting for gas present in the sample at the start of evacuation, is typically less than 0.05 gas fraction. No error bars are shown for the gas fraction results because the established uncertainties are relatively small: 1) the measurement uncertainty for a single analysis is estimated at ~0.01 gas fraction (Section 4.1.4); and 2) replicate analyses for a single S-102 saltcake composite gave <0.03 difference in gas fraction at maximum retention (Gauglitz et al. 1996). The error in the S-102 replicates corresponds to about 6% relative percent difference. These uncertainty measures do not necessarily account for variations in experimental conditions that may occur from sample to sample (e.g., the pressure upset observed in the U-103 upper composite experiment described in Section 4.4.2).

The abscissa values for the center plot of Figure 5.1 are waste strength. For bentonite clays these are the measured shear strength values for gas-free compositions. Both the shear and the tensile strengths of bentonite clay preparations decreased with increasing gas fraction (Gauglitz et al. 1995), and no attempt is made to correct estimated waste strengths for the retained gas fraction in simulated (or actual) wastes. The bentonite clay results demonstrate that the strength of a material influences the gas retention (maximum gas fraction) and release (profile) characteristics. However, because the chemical and physical properties of the actual waste samples are different than those of bentonite clay, clay gas retention and release behavior alone cannot be used as a standard to judge the strength of actual waste samples. To place the actual waste results on the central plot of Figure 5.1, the strength of the actual waste samples must be assigned independent of the bubble shape and other gas retention properties.

The shear strength analyses reported in Section 3 are an obvious source for the A-101, S-106, and U-103 sample strengths for Figure 5.1. However, visual observations of the waste samples as they were being transferred to the retention vessels suggest that the samples, having been

mixed (sheared) to aid in transfer, were considerably weaker than the measured shear strengths (>600 Pa) of the minimally disturbed samples. In each of the samples, the transferred material had a milkshake-like consistency and was sufficiently fluid that it could be poured into the retention vessel. Experience in handling bentonite clay samples of known strengths suggests that a readily pourable material has a shear strength much less than 100 Pa. Accordingly, strengths for the four current-year retention samples were estimated at less than 100 Pa. (However, some rebound in strength is expected after the samples settle two to four weeks prior to the gas retention evacuation experiments.) The error bars in the strength values (center plot of Figure 5.1) for actual waste samples are arbitrary and are intended to indicate considerable uncertainty in these visual estimates. A similar visual approach was used to assign strengths to S-102 sludge and saltcake samples (Gauglitz et al. 1996).

A series of gas retention experiments on bentonite clays of varying strength, including those shown along the bottom of Figure 5.1 and others, is the foundation of the center plot. The clay data are depicted by filled-black circles, and a visually fit line is drawn through the points to represent the trend in maximum gas fraction with strength. The plot shows an increase in maximum gas fraction as the strengths of the clays increase from very weak, water-like consistencies to moderately strong, milkshake-like materials (~50 Pa, maximum void ~0.4). As the strength is increased further, the maximum gas fraction decreases to ~0.3 at the maximum clay strength tested (1040 Pa, consistency of peanut butter). For still stronger materials, it is unknown whether the maximum gas fraction remains near the 0.3 value or whether the retained gas monotonically decreases with increasing strength. Extrapolation of the bentonite clay curve suggests that the latter is most likely. Even so, appreciable gas fractions (~0.2) appear feasible for very strong materials (10 kPa).

The bentonite clay data clearly indicate the correlation of maximum gas retention and gas release characteristics with strength, and the limited actual waste data are generally in good agreement. In the series of actual waste results (A-101, S-106, U-103) in which the nominal strengths of the samples are estimated to be approximately the same, the measured maximum gas fraction varies from ~0.3 to 0.5, including the potentially anomalous U-103 upper composite result (0.3). Without this low value, the SST sample maximum gas fraction range is considerably tighter (0.4–0.5). The bentonite clays of apparently similar strength (~30–70 Pa) also have a maximum gas fraction of about 0.4. In the S-102 samples, where strengths varied by more than an order of magnitude, the trend of decreasing maximum retention with increasing strength lends credence to the correlation of actual SST waste experiments to the clay results. Here again, however, the 0.5 maximum gas fraction in the weakest S-102 sample (~70 Pa) is somewhat higher than the bentonite clay curve in the Figure 5.1 center plot.

Two broadly categorized factors may account for differences in maximum retention among simulated and actual waste samples: 1) variation in maximum retention results at a given strength (i.e., replicate analyses required); and/or 2) a variable in addition to strength (e.g., waste density, particle size distribution, surface tension, or colloidal properties) not accounted for in the model, leading to improper representation of the actual waste strengths through this visual correlation method. While both factors are likely at work, the small variability of replicate analyses for

S-102 saltcake noted above diminish reproducibility as the primary concern. An unaccounted variable seems most likely. In the different waste types it is reasonable to expect that a given gas fraction may have a different impact on the effective strength of the waste because of differences, for example, in interparticle interactions. A more accurate model might result by considering the actual strengths of the material at maximum retention, a difficult task. Further analysis is required to investigate these possibilities with bentonite clay and other well-characterized simulated wastes of various strengths. More directly, an improved method is needed to determine the strength of the in situ gas retention samples.

6.0 References

Agnew SF. 1995. *Hanford Defined Wastes: Chemical and Radionuclide Compositions.* LA-UR-94-2657 Rev 2., Los Alamos National Laboratory, Los Alamos, New Mexico.

Brager HR. 1994. *Summary of Information of Flammable Gas Watch List Tanks.* WHC-EP-0711, Westinghouse Hanford Company, Richland, Washington.

Bredt PR and SM Tingey. 1996. *The Effect of Dilution on the Gas Retention Behavior of Tank 241-SY-103 Waste.* PNL-10893, Pacific Northwest National Laboratory, Richland, Washington.

Bredt PR, SM Tingey, and EH Shade. 1995. *The Effect of Dilution on the Gas-Retention Behavior of Tank 241-SY-101 Waste.* PNL-10781, Pacific Northwest Laboratory, Richland, Washington.

Brevick CH, RL Newell, and JW Funk. 1996. *Historical Tank Content Estimate for the Northeast Quadrant of the Hanford 200 East Area.* WHC-SD-WM-ER-349 Rev. 1-A, Westinghouse Hanford Company, Richland, Washington.

Brevick CH, LA Gaddis, and ED Johnson. 1994. *Supporting Document for the Historical Tank Content Estimate for U Tank Farm.* WHC-SD-WM-ER-325 Rev. 0, ICF Kaiser Hanford Company, Richland, Washington.

Dullien FAL. 1992. *Porous Media: Fluid Transport and Pore Structure.* Academic Press, San Diego.

Field JG, SR Wilmarth, and GL Miller. 1998. *Tank Characterization Report for Single Shell Tank 241-S-106.* HNF-SD-WM-ER-714 Rev. 1, Lockheed Martin Services Inc., Richland, Washington.

Field JG, DE Place, and RD Cromar. 1997. *Tank Characterization Report for Single Shell Tank 241-A-101.* HNF-SD-WM-ER-673 Rev. 0-A, Lockheed Martin Services Inc., Richland, Washington.

Gauglitz PA, LA Mahoney, DP Mendoza, and MC Miller. 1994. *Mechanisms of Gas Bubble Retention.* PNL-10120, Pacific Northwest Laboratory, Richland, Washington.

Gauglitz PA, SD Rassat, MR Powell, RR Shah, and LA Mahoney. 1995. *Gas Bubble Retention and its Effect on Waste Properties: Retention Mechanisms, Viscosity, and Tensile and Shear Strength.* PNL-10740, Pacific Northwest Laboratory, Richland, Washington.

Gauglitz PA, SD Rassat, PR Bredt, JH Konynenbelt, SM Tingey, and DP Mendoza. 1996. *Mechanisms of Gas Bubble Retention and Release: Results for Hanford Waste Tanks 241-S-102 and 241-SY-103 and Single-Shell Tank Simulants.* PNNL-11298, Pacific Northwest National Laboratory, Richland, Washington.

Gauglitz PA and JT Aikin. 1997. *Waste Behavior During Horizontal Extrusion: Effect of Waste Strength for Bentonite and Kaolin/Ludox Simulants and Strength Estimates for Wastes from Hanford Waste Tanks 241-SY-103, AW-101, AN-103, and S-102.* PNNL-11706, Pacific Northwest National Laboratory, Richland, Washington.

Glasscock J. 1993. *Surveillance Analysis Computer System Temperature Database Software Requirements Specification.* WHC-SD-WM-CSRS-007 Rev. 1-A, Westinghouse Hanford Company, Richland, Washington.

Hanlon BM. 1995. *Waste Tank Summary Report for Month Ending August 31, 1995.* WHC-EP-0182-89, Westinghouse Hanford Company, Richland, Washington.

Hanlon BM. 1997. *Waste Tank Summary Report for Month Ending April 30, 1997.* HNF-EP-0182-109, Lockheed Martin Hanford Corporation, Richland, Washington.

Hanlon BM. 1998. *Waste Tank Summary Report for Month Ending January 31, 1998.* HNF-EP-0182-118, Lockheed Martin Services Inc., Richland, Washington.

Johnson GD. 1997. *Strategy for Resolution of the Flammable Gas Safety Issue.* HNF-SD-WM-ER-680, Duke Engineering Services Hanford Company, Richland, Washington.

Johnson GD, WB Barton, JW Brothers, SA Bryan, PA Gauglitz, RC Hill, LR Pederson, CW Stewart, and LM Stock. 1997a. "Evaluation of High-Level Nuclear Waste Tanks Having a Potential Flammable Gas Hazard." *Proceedings of Waste Management 97*, Tucson, Arizona.

Johnson GD, WB Barton, JW Brothers, SA Bryan, PA Gauglitz, RC Hill, LR Pederson, CW Stewart, and LM Stock. 1997b. *Flammable Gas Project Topical Report.* PNNL-11500, Richland, Washington (also published as HNF-SP-1193 Rev. 2).

King CM, LR Pederson, and SA Bryan. 1997. *Thermal and Radiolytic Gas Generation from Tank 241-S-102 Waste.* PNNL-11600, Pacific Northwest National Laboratory, Richland, Washington.

Kupfer MJ, RE Stout, and RT Winward. 1997. *Preliminary Tank Characterization Report for Single Shell Tank 241-U-103.* HNF-SD-WM-ER-712 Rev. 0, Lockheed Martin Services Inc., Richland, Washington.

Mahoney, LA, ZI Antoniak, and JM Bates. 1997. *Composition and Quantities of Retained Gas Measured in Hanford Waste Tanks 241-U-103, S-106, BY-101, and BY-109.* PNNL-11777, Pacific Northwest National Laboratory, Richland, Washington.

Meyer PA, ME Brewster, SA Bryan, G Chen, LR Pederson, CW Stewart, and G Terrones. 1997. *Gas Retention and Release Behavior in Hanford Double-Shell Waste Tanks.* PNNL-11536 Rev. 1, Pacific Northwest National Laboratory, Richland, Washington.

Nguyen QD and DV Boger. 1992. "Measuring the Flow Properties of Yield Stress Fluids." *Ann. Rev. Fluid Mech.*, 24:47-88.

Rassat SD and PA Gauglitz. 1995. *Bubble Retention in Synthetic Sludge: Testing of Alternative Gas Retention Apparatus.* PNL-10661, Pacific Northwest Laboratory, Richland, Washington.

Rassat SD, PA Gauglitz, PR Bredt, LA Mahoney, SV Forbes, and SM Tingey. 1997. *Mechanisms of Gas Retention and Release: Experimental Results for Hanford Waste Tanks 241-AW-101 and 241-AN-103.* PNNL-11642, Pacific Northwest National Laboratory, Richland, Washington.

Remund KM, CM Anderson, and BC Simpson. 1995. *Hanford Single-Shell Tank Grouping Study.* PNL-10749, Pacific Northwest National Laboratory, Richland, Washington.

Shekarriz A, DR Rector, LA Mahoney, MA Chieda, JM Bates, RE Bauer, NS Cannon, BE Hey, CG Linschooten, FJ Reitz, and ER Siciliano. 1997. *Composition and Quantities of Retained Gas Measured in Hanford Waste Tanks 241-AW-101, A-101, AN-105, AN-104, and AN-103.* PNNL-11450 Rev. 1, Pacific Northwest National Laboratory, Richland, Washington.

Stewart CW, ME Brewster, PA Gauglitz, LA Mahoney, PA Meyer, KP Recknagle, and HC Reid. 1996. *Gas Retention and Release Behavior in Hanford Single-Shell Waste Tanks.* PNNL-11391, Pacific Northwest National Laboratory, Richland, Washington.

Swaney SL. 1996. *Single-Shell Tank Leak Stabilization Record.* WHC-SD-RE-TI-178 Rev. 5, Westinghouse Hanford Company, Richland, Washington.

Walker DD, CL Crawford, and NE Bibler. 1994. "Radiolytic Bubble Formation and Level Changes in Simulated High-Level Waste Salts and Sludges - Application to HLW Storage Tanks." *Proceedings of Waste Management 1994*, Tucson, Arizona, pp. 393-396.

WHC. 1996a. *A Safety Assessment of Push-Mode and Rotary-Mode Core Sampling in Flammable Gas Single Shell Tanks: Hanford Site, Richland, Washington.* WHC-SD-WM-SAD-035 Rev. 1, Westinghouse Hanford Company, Richland, Washington.

WHC. 1996b. *A Safety Assessment for Salt Well Jet Pumping Operations in Tank 241-A-101: Hanford Site, Richland, Washington.* WHC-SD-WM-SAD-036 Rev. 0, Westinghouse Hanford Company, Richland, Washington.

Appendix

Gas Retention Data

Table A.1. Gas Retention Data for Tank A-101; Core 154, Segment 5, Sample S97M000176

Date	Time	Solids Layer Height, cm	Total (liquid) Height, cm	Growth Volume, mL	Growth Void Fraction	Pressure, mm Hg
2/20/98	11:39:03	14.40	14.40	0.0	0.000	745.1
	11:58:33	14.45	14.50	0.5	0.007	684.7
	12:24:43	14.50	14.55	0.7	0.010	605.7
	12:55:03	14.60	14.70	1.5	0.021	534.1
	13:08:03	14.60	14.70	1.5	0.021	507.9
	13:48:13	14.90	15.00	3.0	0.040	442.2
	14:37:43	15.10	15.20	4.0	0.053	380.8
	15:01:03	15.30	15.40	5.0	0.065	357.6
	15:25:03	15.40	15.50	5.5	0.071	336.9
	16:16:12	15.70	15.70	6.5	0.083	299.1
	16:31:12	15.80	15.80	7.0	0.088	289.2
	16:53:02	15.90	15.90	7.5	0.094	276.8
	17:35:02	16.10	16.10	8.4	0.105	255.2
	17:59:42	16.35	16.35	9.7	0.119	243.6
	18:16:02	16.40	16.40	9.9	0.122	236.8
	18:53:02	16.60	16.60	10.9	0.132	223.2
	19:21:02	16.70	16.70	11.4	0.138	213.2
	19:44:02	16.90	16.90	12.4	0.148	205.5
	20:06:42	17.10	17.10	13.4	0.158	198.9
	20:36:02	17.20	17.20	13.9	0.163	190.7
	20:59:12	17.40	17.40	14.9	0.172	184.9
	21:22:02	17.60	17.60	15.9	0.182	179.0
	22:01:02	17.80	17.80	16.9	0.191	170.6
	22:23:52	17.90	17.90	17.4	0.195	165.5
	23:11:02	18.30	18.30	19.4	0.213	156.7
	23:59:22	18.40	18.40	19.9	0.217	149.2
2/21/98	0:30:02	18.50	18.50	20.4	0.221	144.1
	1:00:01	18.70	18.70	21.4	0.230	139.3
	1:18:01	19.00	19.00	22.8	0.242	137.1
	1:34:11	19.20	19.20	23.8	0.250	135.4
	2:01:11	19.40	19.40	24.8	0.257	131.3
	2:43:41	19.50	19.50	25.3	0.261	126.7
	3:16:31	19.70	19.70	26.3	0.269	122.5
	3:38:11	19.85	19.85	27.1	0.274	119.4
	3:53:01	19.90	19.90	27.3	0.276	118.6
	4:26:21	20.00	20.00	27.8	0.280	115.0
	4:37:41	20.05	20.05	28.1	0.281	113.6
	4:48:11	20.20	20.20	28.8	0.287	112.6
	5:16:11	20.40	20.40	29.8	0.294	110.6
	5:53:21	20.60	20.60	30.8	0.301	106.8
	6:06:21	20.80	20.80	31.8	0.307	105.8
	6:30:51	20.90	20.90	32.3	0.311	104.1
	7:04:01	21.00	21.00	32.8	0.314	101.9
	7:32:41	21.10	21.10	33.3	0.317	99.0
	7:59:51	21.40	21.40	34.8	0.327	98.0

Table A.1. Gas Retention Data for Tank A-101; Core 154, Segment 5, Sample S97M000176

Date	Time	Solids Layer Height, cm	Total (liquid) Height, cm	Growth Volume, mL	Growth Void Fraction	Pressure, mm Hg
2/21/98	8:30:21	21.80	21.80	36.8	0.339	94.9
	8:58:31	22.00	22.00	37.7	0.345	92.9
	9:29:31	22.40	22.40	39.7	0.357	91.2
	10:02:31	22.60	22.60	40.7	0.362	89.3
	10:42:11	22.60	22.60	40.7	0.362	87.6
	10:45:21	22.40	22.40	39.7	0.357	87.6
	10:55:21	22.30	22.30	39.2	0.354	86.4
	11:07:51	22.00	22.00	37.7	0.345	86.4
	11:29:52	21.60	21.60	35.8	0.333	84.7
	12:00:22	21.45	21.45	35.0	0.328	83.7
	12:30:02	21.40	21.40	34.8	0.327	81.8
	13:30:12	21.30	21.30	34.3	0.324	78.9

Table A.2. Gas Retention Data for Tank S-106; Core 183, Segment 8, Sample S97T000383

Date	Time	Solids Layer Height, cm	Total (liquid) Height, cm	Growth Volume, mL	Growth Void Fraction	Pressure, mm Hg
3/2/98	14:08:02	11.50	11.65	0.0	0.000	746.1
	14:19:22	11.60	11.75	0.5	0.009	692.7
	14:37:12	11.80	11.85	1.0	0.017	609.8
	15:00:02	11.90	11.95	1.5	0.025	528.8
	15:30:12	12.10	12.15	2.5	0.041	449.5
	16:00:02	12.45	12.50	4.2	0.068	391.7
	16:42:21	12.80	12.80	5.7	0.090	331.6
	17:00:21	12.90	12.90	6.2	0.097	311.0
	17:30:11	13.00	13.00	6.7	0.104	281.4
	18:00:31	13.35	13.35	8.4	0.127	257.1
	18:30:21	13.50	13.50	9.1	0.137	238.0
	19:00:50	13.75	13.75	10.4	0.152	220.3
	19:30:10	14.00	14.00	11.6	0.168	205.7
	20:00:00	14.20	14.20	12.6	0.179	191.9
	20:30:10	14.40	14.40	13.6	0.191	180.7
	21:00:00	14.60	14.60	14.6	0.202	170.8
	21:30:40	14.85	14.85	15.8	0.215	160.6
	22:00:29	15.05	15.05	16.8	0.226	152.8
	22:30:09	15.30	15.30	18.0	0.238	146.3
	23:00:19	15.50	15.50	19.0	0.248	139.3
	23:30:09	15.70	15.70	20.0	0.258	132.7
3/3/98	0:00:07	16.00	16.00	21.5	0.271	127.6
	0:30:26	16.20	16.20	22.5	0.280	121.8
	1:00:47	16.50	16.50	23.9	0.293	117.0
	1:32:46	16.85	16.85	25.7	0.308	112.8
	2:00:06	17.00	17.00	26.4	0.314	109.2
	2:30:06	17.25	17.25	27.6	0.324	105.3
	3:00:05	17.50	17.50	28.9	0.334	101.2
	3:30:05	17.70	17.70	29.9	0.341	98.3
	4:00:15	18.00	18.00	31.3	0.352	95.4
	4:30:35	18.20	18.20	32.3	0.359	92.7
	4:53:35	18.50	18.50	33.8	0.370	89.3
	5:15:54	18.70	18.70	34.8	0.376	87.6
	5:45:14	18.95	18.95	36.0	0.385	85.7
	6:14:13	19.20	19.20	37.3	0.393	82.5
	6:45:03	19.50	19.50	38.7	0.402	80.8
	7:16:03	19.70	19.70	39.7	0.408	78.9
	8:00:03	20.00	20.00	41.2	0.417	76.0
	8:30:13	20.30	20.30	42.7	0.426	74.0
	9:00:23	20.60	20.60	44.2	0.434	72.1
	9:15:03	20.90	20.90	45.7	0.442	71.4
	9:35:13	21.30	21.30	47.6	0.452	70.1
	9:41:43	22.00	22.00	51.1	0.470	69.9
	9:45:33	16.00	16.00	21.5	0.271	69.2
	10:05:23	16.00	16.00	21.5	0.271	68.0
	11:00:53	16.00	16.00	21.5	0.271	66.5
	12:27:22	16.10	16.10	22.0	0.276	62.6
	12:47:21	16.10	16.10	22.0	0.276	62.1

Table A.3. Gas Retention Data for Tank U-103; Core 182, Segments 1UH, 1LH, 2UH, and 2LH, Composite S97M000224

Date	Time	Solids Layer Height, cm	Total (liquid) Height, cm	Growth Volume, mL	Growth Void Fraction	Pressure, mm Hg
2/26/98	9:57:03	14.35	14.45	0.0	0.000	755.1
	10:01:03	14.40	14.50	0.2	0.003	707.3
	10:30:38	14.50	14.70	1.2	0.017	477.1
	11:00:19	14.75	14.95	2.5	0.034	325.5
	11:30:29	14.95	15.15	3.5	0.047	245.5
	12:00:09	15.25	15.40	4.7	0.062	198.2
	12:30:39	15.50	15.65	5.9	0.077	165.2
	13:00:09	15.85	15.95	7.4	0.095	142.7
	13:30:09	16.10	16.10	8.1	0.103	125.4
	14:00:29	16.45	16.45	9.9	0.122	110.2
	14:14:09	16.55	16.55	10.4	0.127	105.8
	14:30:49	16.80	16.80	11.6	0.140	100.0
	15:00:59	17.05	17.05	12.8	0.153	91.2
	15:30:09	17.45	17.45	14.8	0.172	83.2
	16:00:09	17.80	17.80	16.5	0.188	77.4
	16:30:09	18.05	18.05	17.7	0.200	71.6
	17:00:39	18.50	18.50	20.0	0.219	66.3
	17:30:29	18.70	18.70	21.0	0.227	64.3
	19:00:48	18.70	18.70	21.0	0.227	64.1
	22:00:38	18.70	18.70	21.0	0.227	63.6
	23:07:48	18.80	18.80	21.4	0.231	63.4
2/27/98	2:00:08	18.80	18.80	21.4	0.231	62.9
	7:00:18	18.90	18.90	21.9	0.236	61.2
	8:38:17	19.00	19.00	22.4	0.240	60.4
	9:30:08	19.05	19.05	22.7	0.242	59.5
	10:00:08	19.05	19.05	22.7	0.242	59.2
	10:02:48	18.40	18.40	19.5	0.215	73.8
	10:06:18	18.70	18.70	21.0	0.227	64.6
	10:11:58	19.05	19.05	22.7	0.242	60.2
	10:30:08	19.15	19.15	23.2	0.245	59.2
	10:38:48	19.15	19.15	23.2	0.246	59.5
	11:00:18	19.20	19.20	23.4	0.248	60.0
	11:15:38	19.40	19.40	24.4	0.255	57.8
	11:29:18	19.55	19.55	25.1	0.261	55.8
	11:39:08	19.90	19.90	26.9	0.274	53.9
	11:42:08	20.15	20.15	28.1	0.283	54.1
	11:42:48	19.55	19.55	25.1	0.261	54.4
	12:15:08	19.70	19.70	25.9	0.267	49.5
	12:25:18	19.85	19.85	26.6	0.272	48.6
	12:28:08	20.20	20.20	28.3	0.285	48.6
	12:29:08	19.60	19.60	25.4	0.263	49.3
	13:00:08	19.55	19.55	25.1	0.261	45.4
	13:54:48	19.00	19.00	22.4	0.240	40.6
	14:50:28	19.40	19.40	24.4	0.255	34.7

Table A.4. Gas Retention Data for Tank U-103; Core 182, Segments 5UH, 5LH, 6UH, and 6LH, Composite S97M000225

Date	Time	Solids Layer Height, cm	Total (liquid) Height, cm	Growth Volume, mL	Growth Void Fraction	Pressure, mm Hg
2/24/98	13:46:38	13.25	13.35	0.0	0.000	745.6
	14:14:07	13.40	13.50	0.7	0.011	469.6
	14:30:07	13.50	13.60	1.2	0.019	376.0
	15:00:17	13.80	13.90	2.7	0.040	274.4
	15:10:57	13.85	13.90	2.7	0.040	250.1
	15:30:07	13.95	13.95	3.0	0.043	215.9
	15:43:07	14.10	14.10	3.7	0.053	197.5
	16:05:08	14.25	14.25	4.5	0.063	173.2
	16:37:16	14.50	14.50	5.7	0.079	145.6
	17:00:56	14.70	14.70	6.7	0.092	131.0
	17:30:16	14.95	14.95	7.9	0.107	116.5
	18:00:47	15.15	15.15	8.9	0.119	103.6
	18:30:16	15.40	15.40	10.1	0.133	94.6
	19:00:56	15.60	15.60	11.1	0.144	86.1
	19:30:06	15.90	15.90	12.6	0.160	79.4
	20:00:06	16.20	16.20	14.1	0.176	73.5
	20:30:16	16.45	16.45	15.3	0.188	68.9
	21:00:16	16.70	16.70	16.6	0.200	65.0
	21:30:26	17.00	17.00	18.1	0.215	60.7
	22:00:26	17.25	17.25	19.3	0.226	57.0
	22:30:36	17.50	17.50	20.5	0.237	53.9
	22:46:16	17.70	17.70	21.5	0.246	51.7
	23:00:06	17.85	17.85	22.3	0.252	51.0
	23:08:36	17.95	17.95	22.8	0.256	49.8
	23:20:16	18.05	18.05	23.3	0.260	48.8
	23:32:36	18.30	18.30	24.5	0.270	47.8
	23:45:46	18.40	18.40	25.0	0.274	46.9
	23:58:26	18.50	18.50	25.5	0.277	45.9
2/25/98	0:12:16	18.55	18.55	25.7	0.280	44.4
	0:26:46	18.70	18.70	26.5	0.286	43.7
	0:42:06	18.95	18.95	27.7	0.295	43.0
	1:14:36	19.20	19.20	28.9	0.304	41.0
	1:31:26	19.40	19.40	29.9	0.312	40.1
	1:49:46	19.55	19.55	30.7	0.317	39.1
	2:08:16	19.85	19.85	32.2	0.327	38.6
	2:28:16	20.00	20.00	32.9	0.332	37.6
	2:49:26	20.15	20.15	33.6	0.337	36.9
	3:20:46	20.25	20.25	34.1	0.340	36.2
	4:13:06	20.35	20.35	34.6	0.344	36.2
	5:00:26	20.35	20.35	34.6	0.344	35.9
	5:30:26	20.35	20.35	34.6	0.344	35.9
	6:00:56	20.40	20.40	34.9	0.345	35.2
	7:20:26	20.50	20.50	35.4	0.349	35.2
	7:43:36	20.70	20.70	36.4	0.355	33.5

Table A.4. Gas Retention Data for Tank U-103; Core 182, Segments 5UH, 5LH, 6UH, and 6LH, Composite S97M000225

Date	Time	Solids Layer Height, cm	Total (liquid) Height, cm	Growth Volume, mL	Growth Void Fraction	Pressure, mm Hg
2/25/98	7:43:56	21.55	21.55	40.6	0.380	31.3
	7:44:16	22.00	22.00	42.8	0.393	29.6
	7:44:56	21.50	21.50	40.3	0.379	27.5
	7:45:36	22.50	22.50	45.3	0.406	26.7
	7:45:56	22.85	22.85	47.0	0.416	27.0
	7:46:06	21.00	21.00	37.8	0.364	26.5
	7:49:06	22.40	22.40	44.8	0.404	22.4
	7:49:36	21.70	21.70	41.3	0.385	23.8
	8:26:06	21.70	21.70	41.3	0.385	23.8
	10:18:06	20.00	20.00	32.9	0.332	23.1
	10:53:26	19.00	19.00	28.0	0.297	22.1
	11:47:46	18.00	18.00	23.0	0.258	22.1
	14:55:26	17.50	17.50	20.5	0.237	19.7

Distribution

No. of
Copies

Offsite

2 DOE Office of Scientific and Technical Information

H. Babad
2540 Cordoba Court
Richland, WA 99352

D. O. Campbell
102 Windham Road
Oak Ridge, TN 37830

P. dEntremont
Westinghouse Savannah River Co.
703-H
Aiken, SC 29802

C. W. Forsberg
Oak Ridge National Laboratory
P.O. Box 2008, MS-6495
Oak Ridge, TN 37831-6495

B. C. Hudson
P.O. Box 271
Lindsborg, KS 67456

J. L. Kovach
P.O. Box 29151
70000 Huntley Road
Columbus, OH 43229

T. S. Kress
102-B Newridge Road
Oak Ridge, TN 37830

Offsite

K. Lang
1041 Cloverleaf Bldg.
1900 Germantown Road
Germantown, MD 20874

T. E. Larson
2711 Walnut St.
Los Alamos, NM 87545

No. of
Copies

3 Los Alamos National Laboratory
P.O. Box 1663
Los Alamos, NM 87545

Attn:	M. E. Brewster	B256
	W. L. Kubic	K575
	C. Unal	K575

D. Meisel
Argonne National Laboratory
9700 S. Cass Avenue
Argonne, IL 60439

D. A. Powers
Sandia National Laboratories
Nuclear Facilities Safety Department
MS-0744
Albuquerque, NM 87185-0744

S. E. Slezak
806 Hermosa NE
Albuquerque, NM 87110

Onsite

4 DOE Richland Operations Office

C. A. Groendyke	S7-54
G. M. Neath	K8-50
G. W. Rosenwald	S7-54
C. L. Sohn	S7-51

29 PHMC Team

S. A. Barker	R2-11
W. B. Barton	R2-11
R. E. Bauer	S7-73
R. J. Cash	S7-73
A. F. Choho	H6-35
K. A. Gasper	G3-21
T. C. Geer	R1-43
J. M. Grigsby	S7-73
D. C. Hedengren	R2-11
D. L. Herting	T6-07
K. M. Hodgson	H0-34

No. of
Copies

T. A. Hu	R2-11
J. R. Jewett	T6-07
G. D. Johnson (5)	S7-73
N. W. Kirch	R2-11
J. G. Kristofzski	R2-12
C. E. Leach	R1-49
J. E. Meacham	S7-73
M. A. Payne	R2-58
J. C. Person	T6-09
D. A. Reynolds	R2-11
L. M. Stock	S7-73
A. B. Webb	A3-37
R. T. Winward	A6-54
A. E. Young	R1-10

No. of
Copies

41 Pacific Northwest National Laboratory

Z. I. Antoniak	K7-15
J. M. Bates	K7-15
S. Q. Bennett	K7-90
P. R. Bredt	P7-25
J. W. Brothers (5)	K9-20
S. A. Bryan	P7-25
S. M. Caley	K6-28
S. V. Forbes	P7-25
P. A. Gauglitz (5)	K6-28
J. L. Huckaby	K6-80
L. A. Mahoney	K7-15
P. A. Meyer	K7-15
L. R. Pederson	K2-44
L. M. Peurrung	K6-28
S. D. Rassat (10)	K6-28
D. E. Rinehart	P7-25
C. L. Shepard	K5-25
C. W. Stewart	K7-15
W. C. Weimer	P7-27
Information Release (5)	K6-06